Thermochemical Properties, $\Delta_f H°(298)$, $S°(298)$, and $C_p°(T)$, for *n*-Butyl and *n*-Pentyl Hydroperoxides and the Alkyl and Peroxy Radicals, Transition States, and Kinetics for Intramolecular Hydrogen Shift Reactions of the Peroxy Radicals

Li Zhu, Joseph W. Bozzelli,* and Lisa M. Kardos

Department of Chemistry and Environmental Science, New Jersey Institute of Technology, Newark, New Jersey 07102

Received: January 15, 2007; In Final Form: April 19, 2007

Alkyl radicals in atmospheric and combustion environments undergo a rapid association with molecular oxygen ($^3O_2$) to form an alkyl peroxy radical (ROO•). One important reaction of these peroxy radicals is the intramolecular H-shift (intramolecular abstraction) to form a hydroperoxide alkyl radical (R′•COOH), where the hydroperoxide alkyl radical may undergo chemical activation reaction with O_2 and result in chain branching at moderate to low temperatures. The thermochemistry and trends in kinetic parameters for the hydrogen shift reactions from each carbon (4−8-member-ring TST's) in *n*-butyl and *n*-pentyl peroxy radicals (CCCCOO• and CCCCCOO•) are analyzed using density functional and ab initio calculation methods. Thermochemical properties, $\Delta_f H°$(298 K), C−H bond energies, $S°$(298 K), and $C_p°(T)$ of saturated linear C4 and C5 aliphatic peroxides (ROOH), as well as the corresponding hydroperoxide alkyl radicals (R′•COOH), are determined. $\Delta_f H°$(298 K) are obtained from isodesmic reactions and the total energies of the CBS-QB3 and B3LYP computational methods. Contributions to the entropy and the heat capacity from translation, vibration, and external rotation are calculated using the rigid-rotor-harmonic-oscillator approximation based on the CBS-QB3 frequencies and structures. The results indicate that pre-exponential factors, $A(T)$, decrease with the increase of the ring size (4−8-member-ring TS, H-atom included). The $\Delta H^‡$ for 4-, 5-, 6-, and 7-member rings in *n*-butyl (and *n*-pentyl) peroxy are 40.8 (40.8), 31.4 (31.5), 20.5 (20.0), 22.6-p (19.4) kcal mol^{-1}, respectively. The $\Delta H^‡$ for the 8-member ring in *n*-pentylperoxy is 23.8-p kcal mol^{-1}, All abstractions are from secondary (−CH_2−) groups except those marked (-p), which are from primary sites. Enthalpy and barrier values from the B3LYP/6-311++G(2d,p) and BHandHLYP/6-311G(d,p) methods are compared with CBS-QB3 results. The B3LYP results show good agreement with the higher level CBS-QB3 calculation method; the BHandH barriers for the intramolecular peroxy H-shifts are not acceptable.

1. Introduction

Thermochemical properties and kinetic parameters of peroxy hydrocarbon and hydroperoxide alkyl radicals are important in atmospheric chemistry of hydrocarbons, and they are strongly linked to the ignition of hydrocarbons at low to moderate temperatures (up to 1100 K). These reactions are also used to explain the negative temperature regime in the oxidation and ignition HCCI engines.[1] These peroxy and hydroperoxide alkyl radicals are reactive species that can be monitored by their broad banded UV absorption; but this is often complicated by absorption from other peroxy radicals or hydroperoxide species, making identification and experimental studies difficult. The atmospheric and combustion chemistry of peroxy radicals is initiated by active radicals (e.g., hydroxyl) in abstraction of H-atoms from hydrocarbons. The alkyl radicals then undergo association reaction with an oxygen molecule to form an alkyl peroxy radical (ROO•). One of the reaction pathways of this peroxy radical is to undergo the intramolecular H-abstraction to form a hydroperoxide alkyl radical (R•OOH). Bozzelli and Sheng have recently shown that these hydroperoxide alkyl radicals can further react with a second O_2, where both chemical activation and stabilized adducts lead to several chain-branching paths.[2] The importance of this chain branching has been verified by detailed modeling and sensitivity results on the negative temperature dependence of propane oxidation.[3]

The intramolecular hydrogen transfer rate constant involving a 5-member-ring transition state structure for $CH_3CH_2OO• \rightarrow C•H_2CH_2OOH$ was reported by Baldwin, Pickering, and Walker as $A = 10^{13.3}\pm^{0.6}$ s^{-1} and $E_a = 34.3 \pm 2.4$ kcal mol^{-1} using experiments on final product profiles between 600 and 800 K, combined with a multifaceted equilibrium and kinetic analysis.[4] These landmark studies employed complex kinetic analysis and involved formation of the stabilized peroxy radical, intramolecular hydrogen transfer, and subsequent reaction of the hydroperoxide alkyl radical to observed products. They utilized thermochemistry for equilibrium constants of the peroxy formation reaction and assumptions requiring some reverse paths to be negligible. In similar experiments, Baldwin, Igham, and Walker determined the rate constant for 1,5-intramolecular hydrogen transfer in neopentane, $C_3CCOO• \rightarrow C_2C(C•)COOH$, as $A = 1.2 \times 10^{13}$ s^{-1} and $E_a = 28.7$ kcal mol^{-1} (a 6-member-ring TS). They correctly noted that the Arrhenius factors should decrease with the increasing ring size, because there is a loss of entropy as additional internal rotations are restricted in the transition state structures.[5]

Wagner, Slagle, Sarzynski, and Gutman studied 5-member-ring TSTs' reaction of $C_2H_5 + O_2$ flow experiments with

* Corresponding author. Phone: (973) 596 3459. Fax: (973) 642 7170. E-mail: bozzelli@adm.njit.edu.

10.1021/jp070342s CCC: $37.00
Published on Web 06/22/2007

molecular beam sampling into a photoionization mass spectrometer, and they utilized RRKM theory for analysis.[6] The barrier height for $CH_3CH_2OO^\bullet \rightarrow C^\bullet H_2CH_2OOH$ was determined to be 30.5 at 0 K to explain the observed ethylene product formation from the $C^\bullet H_2CH_2OOH \rightarrow C_2H_4 + HO_2$ path.

Quelch, Gallo, Shen, Xie, Schaefer, and Moncrieff reviewed the literature on intramolecular hydrogen transfer reactions in 1994.[7] They also used several different calculation methods on the ethyl peroxy radical, to find two distinct, but energetically proximate intramolecular transition states involving movement of the methyl H-atom to the peroxy oxygen radical site. One was a $^2A''$ electronic state (C_s symmetry) linked to $CCOO^\bullet \rightarrow [CH_2CH_2...HO_2] \rightarrow C_2H_4 + HO_2$ (HO_2 molecular elimination). The second path is a ^2A (no symmetry) linked to the hydrogen transfer reaction of $CCOO^\bullet \rightarrow C^\bullet H_2CH_2OOH$. At their best level of theory, DZP CCSD(T), the $^2A''$ and ^2A TST structures were 35.0 and 39.6 kcal mol^{-1} above the CH_3CH_2OO adduct, respectively, and 5 kcal mol^{-1} higher than the data of Wagner et al.

The reaction of $C_2H_5 + O_2$ was further studied using computational chemistry by Ignatyev, Xie, Allen, and Schaefer in 1997 using BLYP, B3LYP, and BHLYP DFT methods.[8] Their comparison with experimental and high-level coupled cluster results suggested that B3LYP method was the superior DFT method for this system. They reported the energy for the TS of $CH_3CH_2OO^\bullet$ isomerization to $C^\bullet H_2CH_2OOH$ was 8.0 kcal mol^{-1} higher than the energy of the $C_2H_5 + O_2$ reactant set, which corresponds to about 7 kcal mol^{-1} higher than the barrier measured in the Wagner et al. experiment. However, they found a lower energy (29 kcal mol^{-1}), direct HO_2 molecular elimination path that explains the ethylene formation in the Wagner et al. (Gutman group) experiments.[6]

The oxidation paths of *n*-butane was studied in 1997 by Jungkamp, Smith, and Seinfeld[9] at the CBS-lq//B3LYP/6-31G(d,p) level. The principal pathways following formation of the 1-butyl radical reaction with O_2 was found to be $CCCC^\bullet + O_2 \rightarrow CCCCOO^\bullet \rightarrow CC^\bullet CCOOH$, where the $\Delta H^\ddagger$ for the 6-member-ring intramolecular H-abstraction was 20.34 kcal mol^{-1}. This value was reported to be 5.1 kcal mol^{-1} lower than the 7-member-ring H-abstraction path, $CCCCOO^\bullet \rightarrow C^\bullet CCCOOH$. Curran et al.[10] evaluated literature on intramolecular H-shift reactions, including ring strain energies and listed pre-exponential and barrier versus number of atoms in the cyclic TS structure for consistency in their model of heptane oxidation.

Chan, Hamilton, and Pritchard calculated rate constants for intramolecular H-abstractions of alkyl peroxy radicals using the BHandHLYP/6-311G(d,p) density functional method.[11] The H-abstraction reactions they reported include (1) the *n*-pentyl peroxy radical where H-abstraction can occur for each of the five carbon atoms, (2) the $CH_3(CH_2)_nOO^\bullet$ series ($n = 0-3$) and the three isomeric pentylperoxy radicals, $(CH_3)_3CCH_2OO^\bullet$, $C_2H_5(CH_3)CHCH_2OO^\bullet$, and $(CH_3)_2CHCH_2CH_2OO^\bullet$ (H on the italicized carbon is abstracted). Chan et al. obtained the pre-exponential *A*-factor and $\Delta H^\ddagger$ for the reactions and compared their data with literature values,[5,12,13] where torsion frequencies were used for internal rotor contributions. They reported a decreasing trend in the pre-exponential factor with increase ring size in the TS from (1,4p) to (1,8p). The log *A* (pre-exponential) values decreased from 13.2 to 11.2 s^{-1}, and the $\Delta H^\ddagger$ also decreases with increased ring size. The $\Delta H^\ddagger$ for abstraction from a secondary carbon was less than for a primary C−H, and abstraction from a tertiary carbon was lower than that from a secondary carbon for comparable TST ring size. Chan et al. concluded that the average difference between the BHandH values for activation energies and those derived from experiment is ca. 7.2 kcal mol^{-1}. They concluded that the BHandH activation energies, reduced by ca. 6.0 kcal mol^{-1} (25 kJ mol^{-1}), resulted in acceptable rate constants for use in models.

Sheng et al. used CBSQ calculations and extensive modeling of literature data on ethyl radical oxidation of Kaiser to determine a high-pressure rate constant for the H-shift reaction in $C_2H_5OO^\bullet$ to $C^\bullet H_2CH_2OOH$ (5-member-ring TS including the H-atom) fitted to be $7.90 \times 10^6 T^{1.79} \exp(-35820/RT)$ s^{-1} over a temperature range 300−2000 K.[14] Cartensen, Naik, and Dean have calculated a similar high-pressure limit rate constant in 2005 for this reaction as $A = 1.92 \times 10^{12}$ s^{-1} and $\Delta H^\ddagger = 35.0$ kcal mol^{-1}.[15] Bozzelli and Sheng[2] also calculated the enthalpy barrier $\Delta H^\ddagger$ for H-shift for a similar 4-member-ring reaction, $HOOCH_2CH_2OO^\bullet \rightarrow HOOCH_2C^\bullet HOOH$, which rapidly dissociates (no barrier, exothermic) to $HOOCH_2CHO + OH$, to be 29.72 kcal mol^{-1} at the CBS-Q//B3LYP/6-31G(d,p) level, which is significantly lower than the isomerization barrier of ethyl−peroxy to hydroperoxy−ethyl, i.e., 36.36 kcal mol^{-1}. The high-pressure limit rate constant for the H-shift in the *tert*-butyl peroxy radical ($C_3COO^\bullet \rightarrow C_2C(C^\bullet)OOH$, 5-member ring) was calculated to be $1.44 \times 10^{10} T^{0.808} \exp(-32760/RT)$ and $3.97 \times 10^9 T^{1.043} \exp(-32060/RT)$ s^{-1} at the CBS-lq//MP2(full)/6-31G(d) and CBS-lq//B3LYP/6-31G(d) levels, respectively.[16]

DeSain et al. reported on experiments of the ethyl and propyl + O_2 systems between 296 and 700 K, and they modeled species profiles of several observed major products.[17] The enthalpy barriers $\Delta H^\ddagger$ for $C_2H_5OO^\bullet$ reaction to $C^\bullet COOH$ and to $[CH_3C^\bullet HOOH]^* \rightarrow$ fast $\rightarrow CH_3CHO + OH$ was reported as 37.0 and 42.1 kcal mol^{-1}, respectively. The $\Delta H^\ddagger$'s for the propyl peroxy radical ($CCCOO^\bullet$) reaction to $CC^\bullet COOH$ and to $C^\bullet CCOOH$ were reported as 33 and 23 kcal mol^{-1}, respectively. The $\Delta H^\ddagger$ for the isopropyl 5-member-ring H-transfer ($CC(C)OO^\bullet$ to $CC(C^\bullet)OOH$) was reported as 34 kcal mol^{-1}.

The conformer energies, statistical distribution, and unimolecular decomposition pathways for the *n*-propylperoxy radical have been calculated at three levels of theory by Merle et al.[18] They demonstrate that CBS-QB3 calculations on the CCC−OO bond energy are in good agreement with experiment data. They also find that B3LYP/6-31+G(d,p) transition state and reaction energies are in very good agreement with the CBS-QB3 values, where MPW1K/6-31+G(d,p) provides transition state energies that are significantly (3−6 kcal mol^{-1}) higher than the CBS-QB3 values. At room temperature, all five rotamers of $CCCOO^\bullet$ are expected to be present, in agreement with cavity ringdown spectroscopy (CRDS) experiments. At the CBS-QB3 level, the largest energy difference between the five rotamers was only 0.6 kcal mol^{-1}.

The choice of calculation methods, B3LYP with various basis sets, G3MP2, and CBS-QB3, was reported to have a significant effect on the results of condensed-phase intramolecular H-abstraction, as studied by Pfaendtner, Yu, and Broadbelt.[19] They reported that B3LYP/6-311+G(d,p) offers a good compromise between speed and accuracy, though CBS-QB3 is the best when feasible. Their study further probed the impact in the size of the cyclic transition state ring on A and $\Delta H^\ddagger$ and an Evans−Polanyi relationship was observed for the 1,5-hydrogen shift (6-member ring with the H included) series.

This study presents a systematic thermochemical and kinetic parameter analysis on the intramolecular H-abstraction reactions for 4−8-member-ring transition states in *n*-butyl and *n*-pentyl peroxy radicals. The trends of rate constant with the size of the ring and the primary, secondary, or peroxy nature of the carbon bonded to the H-atom abstracted are also delineated. The C−H

TABLE 1: Relative Energies of Different Isomers at Different Calculation Levels[a]

species	isomer ID no.	dihedral angles[b] (deg)	B3LYP/6-31G(d,p)// B3LYP/6-31G(d,p)	B3LYP/6-311++G(2d,p)// B3LYP/6-31G(d,p)	CBS-QB3
CCCCOOH	A (zigzag, TTT)	CCCC = 180 CCCO = 180 CCOO = 176 HOOC = 112	0	0	0
	B (TGG′)	CCCC = 176 CCCO = 75 CCOO = −80 HOOC = 124	0.78	1.74	1.46
	C (TGT)	CCCC = 179 CCCO = 64 CCOO = 178 HOOC = 111	−0.18	0.06	−0.15
	D (used, TGG)	CCCC= −178 CCCO = 60 CCOO = 71 HOOC = −118	−0.53	0.28	−0.14
CCCCOO•	A (zigzag, TTT)	CCCC = 180 CCCO = 180 CCOO = 180	0	0	0
	B (TGT)	CCCC = 180 CCCO = 66 CCOO = −176	−0.29	−0.12	−0.33
	C (used, TGG)	CCCC = −179 CCCO = 63 CCOO = 71	−0.69	−0.14	−0.65
C•CCCOOH	A (zigzag, TTT)	CCCC = 180 CCCO = 180 CCOO = 176 HOOC = 112	0	0	0
	B (GGG)	CCCC = 68 CCCO = 62 CCOO = 71 HOOC = −121	−0.92	−0.09	−0.62
	C (TTG)	CCCC = 178 CCCO = 178 CCOO = 71 HOOC = −117	−0.65	−0.19	−0.26
	D (used, TGG)	CCCC = −176 CCCO = 60 CCOO = 71 HOOC = −119	−1.09	−0.37	−0.76
	E (G′GG)	CCCC = −75 CCCO = 51 CCOO = 64 HOOC = −100	−1.09	0.45	−0.64
CC•CCOOH	A (zigzag, TTT)	CCCC = −158 CCCO = −177 CCOO = 176 HOOC = 111	0	0	0
	B (TGT)	CCCC = 165 CCCO = 65 CCOO = 179 HOOC = 111	−0.18	0.04	−0.17
	C (used, TGG)	CCCC = 167 CCCO = 58 CCOO = 70 HOOC = −114	−0.82	−0.05	−0.54
	D (TG′G)	CCCC = 158 CCCO = −67 CCOO = 78 HOOC = −81	−0.88	0.47	0.03
CCC•COOH	A (TGT)	CCCC = 158 CCCO = 76 CCOO = 179 HOOC = 109	0	0	0
	B (TGT)	CCCC = 160 CCCO = 71 CCOO = −174 HOOC = −109	−0.16	−0.13	−0.15
	C (TG′T)	CCCC = −158 CCCO = −76 CCOO = −179 HOOC = −109	−0.01	0	0

TABLE 1: Continued

species	isomer ID no.	dihedral angles[b] (deg)	B3LYP/6-31G(d,p)// B3LYP/6-31G(d,p)	B3LYP/6-311++G(2d,p)// B3LYP/6-31G(d,p)	CBS-QB3
CCC•COOH (cont'd)	D (TGG)	CCCC = −154 CCCO = 60 CCOO = 72 HOOC = −97	−0.30	0.19	−0.23
	E (used, TG′G)	CCCC = −162 CCCO = −98 CCOO = 69 HOOC = −112	−0.51	0.11	−0.26
	F (GG′G)	CCCC = 96 CCCO = −116 CCOO = 69 HOOC = −104	−0.54	0.66	0.02
$TnC_4 14P_{peroxy}$	A	CCCC = 67 CCCO = −175 CCOO = 117	0	0	0
	B	CCCC = −178 CCCO = −173 CCOO = 116	−0.40	−0.48	−0.18
	C (used)	CCCC = 176 CCCO = −53 CCOO = 116	−0.67	−0.32	−0.54
$TnC_4 15S$	A	CCCC = 170 CCCO = −148 CCOO = 46	0	0	0
	B	CCCC = −74 CCCO = −148 CCOO = 46	0.45	0.54	0.30
	C (used)	CCCC = 165 CCCO = −77 CCOO = −46	−0.12	0.03	−0.44
$TnC_4 16S$	A (used)	CCCC = −74 CCCO = −148 CCOO = 46	0	0	0
	B	CCCC = −85 CCCO = −54 CCOO = 69	−0.19	−0.05	0.12
$TnC_4 17P$	A	CCCC = −81 CCCO = 30 CCOO = 58	0	0	0
	B (used)	CCCC = −66 CCCO = 66 CCOO = −79	−1.50	−1.57	−0.95

[a] 298 K, ZPVE and thermal correction (0−298 K) are included; [b] At B3LYP/6-31G(d,p) level.

bond energy on a peroxy carbon is estimated to be several kcal mol^{-1} lower than that for a secondary C_s−H due to resonance, and the kinetics involving this peroxy carbon C−H bond are different from that of a secondary HC radical.

Thermochemical parameters of the reactants and products (ROO• and R′•OOH) as well as the parent hydroperoxides are determined. Calculation methods include density functional B3LYP/6-31G(d,p), B3LYP/6-311++G(2d,p)//B3LYP/6-31G(d,p), BHandHLYP as used by Pritchard's group, and the composite CBS-QB3 method. The CBS-QB3 method is recommended in this work. Comparisons between the methods suggest the B3LYP method is acceptable for elementary kinetic parameters on these intramolecular H-shift reactions (involving peroxide or peroxy moieties). Isodesmic work reactions are used and recommended for enthalpy values of the reactants and products.

2. Nomenclature for Reactions

The nomenclature often used for the H-shift reactions is (1,3s), (1,5p), (1,5t), etc., where the second number indicates the number of heavy atoms in the transition state ring (not inclusive of the H-atom) and s and p indicate the type of carbons whose H is abstracted, primary or secondary. As an example CCOO• → C•COOH is a (1,4p) reaction; the transition state has a 5-member ring that includes the H, and 4 heavy atoms (CCOO) are in the TS structure.

We implement a nomenclature to include the reactions resulting from the carbon bonded to the peroxy group. (The C−H on this peroxy carbon has a lower bond energy than a normal secondary C−H, and this is important in considering the reactions of a second O_2 with the alkyl radical formed in these H-atom transfer reactions.) As an example, the transition state in CCCCOO• → [CCCC•OOH] (fast) → CCCC═O + OH is identified as $TnC_4 14P_{perox}$. Here T represents transition state, nC_4 is *n*-CCCC, 1 represents the position of the OO group (on the first carbon), subscript 4 is the number of atoms in the ring where the shifting H-atom is counted, and P_{perox} identifies the environment of the carbon from which the H-atom is abstracted. $TnC_4 15S$ represents abstraction from a secondary alkyl carbon in the nC_4 system, with a 5-member-ring transition state. $TnC_4 17P$ represents abstraction from a primary alkyl carbon in the nC_4 system, with 7-member-ring transition state.

The reactions studied in this work include:

$$CCCCOO^{\bullet} \rightarrow (TnC_4 14P_{perox}) \rightarrow [CCCC^{\bullet}OOH]^* \xrightarrow{fast} CCCC{=}O + OH \quad (R1)$$

$$CCCCOO^{\bullet} \rightarrow (TnC_4 15S) \rightarrow CCC^{\bullet}COOH \quad (R2)$$

$$CCCCOO^{\bullet} \rightarrow (TnC_4 16S) \rightarrow CC^{\bullet}CCOOH \quad (R3)$$

$$CCCCOO^{\bullet} \rightarrow (TnC_4 17P) \rightarrow C^{\bullet}CCCOOH \quad (R4)$$

$$CCCCCOO^{\bullet} \rightarrow (TnC_5 14P_{perox}) \rightarrow [CCCCC^{\bullet}OOH]^* \xrightarrow{fast} CCCCC{=}O + OH \quad (R5)$$

$$CCCCCOO^{\bullet} \rightarrow (TnC_5 15S) \rightarrow CCCC^{\bullet}COOH \quad (R6)$$

$$CCCCCOO^{\bullet} \rightarrow (TnC_5 16S) \rightarrow CCC^{\bullet}CCOOH \quad (R7)$$

$$CCCCCOO^{\bullet} \rightarrow (TnC_5 17S) \rightarrow CC^{\bullet}CCCOOH \quad (R8)$$

$$CCCCCOO^{\bullet} \rightarrow (TnC_5 18P) \rightarrow C^{\bullet}CCCCOOH \quad (R9)$$

3. Computational Methods

The calculations were performed using the Gaussian 98 and 03 programs. The structure of each reactant, product, and transition state structure is fully optimized at the B3LYP/6-31G(d,p) level of theory. Harmonic vibration frequencies, zero-point vibration energies (ZPVE), and hindered internal rotor potentials are computed at the same level. Curtiss et al.[20] report that B3LYP/6-31G(d,p) provides a highly accurate structure for compounds with elements up to atomic number 10. Durant[21,22] has compared density functional calculations BHandH and B3LYP with MP2 and Hartree−Fock methods for the geometry and vibration frequencies. He reported that these B3LYP density functional methods provided an improved geometry and vibration frequencies, relative to MP2 at reduced computation expense. Petersson[23] has recommended use of B3LYP or BLYP for the geometry and the vibration frequencies in several of his CBS calculation methods. It has also been shown that for these hydroperoxides and peroxy radicals, B3LYP/6-31G(d,p) yields reasonably accurate results for enthalpies of formation when isodesmic reactions are used.[24,25]

The B3LYP/6-311++G(2d,p) method is used to obtain improved DFT level energies, single point energies, based on the optimized B3LYP/6-31G(d,p) structures. The BHandHLYP/6-311G(d,p) method is also used so that we may directly compare data with ref 11 and further evaluate the method.

We use CBS-QB3 calculations to obtain improved accuracy and to determine which density functional method is more appropriate for the thermochemical and kinetic parameter calculations. The CBS-QB3 composite method consists of four calculation steps: (1) B3LYP/6-311G(2d,d,p) level for the geometry optimization and frequencies, (2) CCSD(T)/6-31+G-(d′) energy, (3) MP4SDQ/CBSB4 energy, and (4) MP2/CBSB3 with CBSExtrap = (NMin=10,MinPop).

3.1. $\Delta_f H°$(298K) of Reactants, Products, and Relative Enthalpy of Transition States Structures. Standard enthalpies of formation for reactants and products are obtained using total energies obtained by the B3LYP/6-31G(d,p), B3LYP/6-311++G-(2d,p)//B3LYP/6-31G(d,p), and CBS-QB3 calculation methods and isodesmic reaction analysis. The calculated total energy at B3LYP/6-311++G(2d,p)//B3LYP/6-31G(d,p) is corrected by the ZPVE, which is scaled by 0.9806 for B3LYP/6-31G(d,p) level, as recommended by Scott and Radom.[26] Thermal corrections from 0 to 298 K are calculated to estimate total enthalpies at 298 K.

The following isodesmic reactions are selected to determine $\Delta_f H°$(298 K) of the target (in italics and bold) species.

$$\textit{n-}\boldsymbol{C_4H_9OOH} + n\text{-}C_3H_8 \rightarrow n\text{-}C_3H_7OOH + n\text{-}C_4H_{10} \quad (Ra)$$

$$\textit{n-}\boldsymbol{C_4H_9OO^{\bullet}} + n\text{-}C_3H_8 \rightarrow n\text{-}C_3H_7OO^{\bullet} + n\text{-}C_4H_{10} \quad (Rb)$$

$$\textit{n-}\boldsymbol{C^{\bullet}H_2CH_2CH_2CH_2OOH} + n\text{-}C_3H_7OOH \rightarrow C^{\bullet}H_2CH_2CH_2OOH + n\text{-}C_4H_9OOH \quad (Rc)$$

$$\textit{n-}\boldsymbol{CH_3C^{\bullet}HCH_2CH_2OOH} + n\text{-}C_3H_7OOH \rightarrow CH_3C^{\bullet}HCH_2OOH + n\text{-}C_4H_9OOH \quad (Rd)$$

$$\textit{n-}\boldsymbol{CH_3CH_2C^{\bullet}HCH_2OOH} + n\text{-}C_3H_7OOH \rightarrow CH_3C^{\bullet}HCH_2OOH + n\text{-}C_4H_9OOH \quad (Re)$$

$$\textit{n-}\boldsymbol{C_5H_{11}OOH} + n\text{-}C_3H_8 \rightarrow n\text{-}C_3H_7OOH + n\text{-}C_5H_{12} \quad (Rf)$$

$$\textit{n-}\boldsymbol{C_5H_{11}OO^{\bullet}} + n\text{-}C_3H_8 \rightarrow n\text{-}C_3H_7OO^{\bullet} + n\text{-}C_5H_{12} \quad (Rg)$$

$$\textit{n-}\boldsymbol{C^{\bullet}H_2CH_2CH_2CH_2CH_2OOH} + n\text{-}C_3H_7OOH \rightarrow C^{\bullet}H_2CH_2CH_2OOH + n\text{-}C_5H_{12}OO \quad (Rh)$$

$$\textit{n-}\boldsymbol{CH_3C^{\bullet}HCH_2CH_2CH_2OOH} + n\text{-}C_3H_7OOH \rightarrow CH_3C^{\bullet}HCH_2OOH + n\text{-}C_5H_{12}OOH \quad (Ri)$$

$$\textit{n-}\boldsymbol{CH_3CH_2C^{\bullet}HCH_2CH_2OOH} + n\text{-}C_3H_7OOH \rightarrow CH_3C^{\bullet}HCH_2OOH + n\text{-}C_5H_{12}OOH \quad (Rj)$$

$$\textit{n-}\boldsymbol{CH_3CH_2CH_2C^{\bullet}HCH_2OOH} + n\text{-}C_3H_7OOH \rightarrow CH_3C^{\bullet}HCH_2OOH + n\text{-}C_5H_{12}OOH \quad (Rk)$$

$$\textit{n-}\boldsymbol{C_3H_7CH{=}O} + C_2H_6 \rightarrow CH_3CH{=}O + n\text{-}C_4H_{10} \quad (Rl)$$

$$\textit{n-}\boldsymbol{C_4H_9CH{=}O} + C_2H_6 \rightarrow CH_3CH{=}O + n\text{-}C_5H_{12} \quad (Rm)$$

$\Delta_f H°$(298 K) of the transition states are calculated as the sum of the $\Delta_f H°$(298 K) of reactant and the energy difference between TS and reactant at the respective B3LYP/6-31G(d,p), B3LYP/6-311++G(2d,p)//B3LYP/6-31G(d,p), and CBS-QB3 levels.

3.2. Rotational Conformers. Rotational conformers are studied to determine the lowest energy conformer and enthalpy values, as well as the S and C_p contributions. Because each species (with exclusion of two of the transition states) has one or more internal rotors, it can have several different rotational conformers. The existence of relatively low-energy rotation conformers and transitions through internal rotation barriers between the conformers usually has significant effects on the entropy value of the appropriate molecule, radical, or transition state. As entropy is critical to the pre-exponential factor in kinetics, we evaluate the rotation conformers for each internal rotor in each radical or transition state to calculate the $S°$(298 K) and $C_p°(T)$ ($300 \leq T/K \leq 1500$) values of each species. Each reactant, product, or TS has one or more internal rotors, except $TnC_4$17P and $TnC_5$18P, which have no internal rotor.

TABLE 2: Calculated $\Delta_f H°(298)$ (kcal mol^{-1}) via Isodesmic Work Reactions[a]

isodesmic reactions	target species	B3LYP/6-31G(d,p)// B3LYP/6-31G(d,p)	B3LYP/6-311++G(2d,p)// B3LYP/6-31G(d,p)	CBS-QB3
Ra	CCCCOOH	−50.20	−49.44	**−49.74**
Rb	CCCCOO•	−17.08	−17.09	**−17.14**
Rc	C•CCCOO	0.46	−0.33	**−0.05**
Rd	CC•CCOO	−2.65	−3.11	**−3.14**
Re	CCC•COO	−1.79	−2.50	**−2.20**
Rf	CCCCCOOH	−55.31	−54.57	**−54.96**
Rg	CCCCCOO•	−22.19	−22.26	**−22.37**
Rh	C•CCCCOO	−4.68	−5.51	**−5.21**
Ri	CC•CCCOO	−7.97	−7.42	**−8.66**
Rj	CCC•CCOO	−7.65	−8.19	**−8.13**
Rk	CCCC•COO	−7.30	−7.35	**−7.35**
Rl	CCCC=O	−50.32	−49.72	**−49.82**[b]
Rm	CCCCC=O	−55.43	−54.88	**−54.99**[c]

[a] Values in bold are recommended here; [b] This value is calculated as −50.0 ± 0.7 by da Silva and Bozzelli[38] using isodesmic reaction at CBS-APNO, G3, and G3B3; [c] This value is calculated as −54.1 ± 0.5 by da Silva and Bozzelli[38] using isodesmic reaction at CBS-APNO, G3, and G3B3; they finally chose to use the experimental value of −54.61 by Pedley et al.[39]

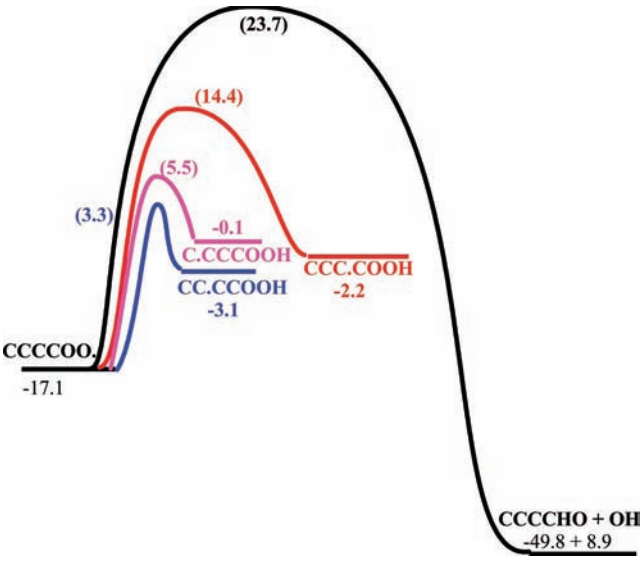

Figure 1. Potential Energy Diagram for intramolecular H-atom abstraction reactions in the *n*-butyl peroxy radical, CCCCOO•, at the CBS-QB3 level. Data are enthalpies of formation $\Delta_f H°$ at 298 K and ($\Delta H^{\ddagger}$) (units: kcal mol^{-1}).

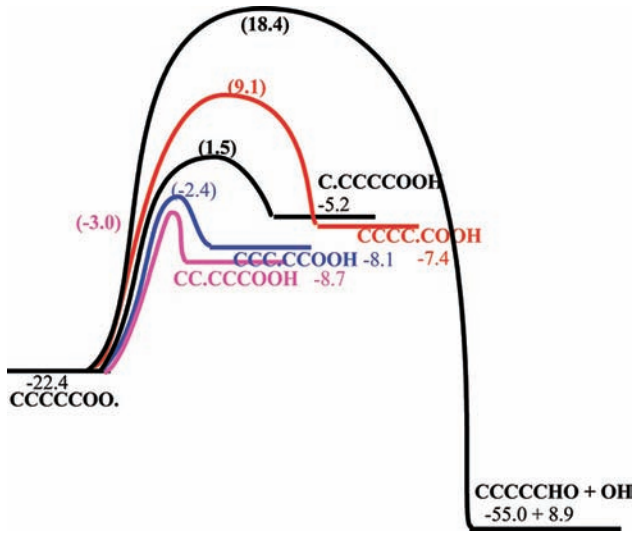

Figure 2. Potential energy diagram for intramolecular H-atom abstraction reactions in the *n*-pentyl peroxy radical, CCCCCOO•, at the CBS-QB3 level. Data are enthalpies of formation $\Delta H°_f$ at 298 K and ($\Delta H^{\ddagger}$) (units: kcal mol^{-1}).

We use the lowest energy rotational isomer as determined at the CBS-QB3 level. The internal rotor analysis described below calculates the entropy and $C_p(T)$ contributions for the rotamers.

3.3. S°(298 K), and C_p°(T) (300 ≤ T/K ≤ 1500) and the Contributions of Hindered Internal Rotations to the Thermochemical Properties. Contributions to $S°$(298 K) and $C_p°(T)$ (300 ≤ T/K ≤ 1500) from translation, vibration, and external rotation (TVR) of each species are obtained using the rigid-rotor-harmonic-oscillator approximation for the frequencies, along with moments of inertia based on the optimized CBS-QB3 structure. A computer program "SMCPS"[27] has been written for purposes of these calculations. The torsion frequencies (corresponding to the internal rotational barrier whose barrier are less than 5 kcal mol^{-1}) are not included in the TVR calculations. The contributions to standard entropy and heat capacities of TS species from translation, vibration, and external rotation are calculated the same way as the non-TS species, except that the imaginary frequency is excluded.

3.4. Internal Rotor Analysis. Contributions to entropy and heat capacities for internal rotations that have barriers below 5 kcal mol^{-1} are determined using direct integration over the energy levels of the internal rotation potential, where the curves were determined at the B3LYP/6-31G(d,p) level. The replaced torsion frequencies are marked and selection discussed in the supplementary table (S2). A program "ROTATOR"[27,28] is used for calculation of the internal rotor energy levels and conformer contributions to $S°$(298 K) and $C_p°(T)$. The method employs expansion of the hindrance potential in the Fourier series (eq I), calculation of the Hamiltonian matrix in the basis of wave functions of free internal rotors, and subsequent calculation of energy levels by direct diagonalization of the Hamiltonian matrix.[29−31] The internal rotor potential calculated at discrete torsion angles is represented by a truncated Fourier series:

$$V(\Phi) = a_0 + a_i \cos(i\Phi) + b_i \sin(i\Phi) \qquad i = 1, 2, 3, \ldots \quad \text{(I)}$$

Values of the coefficient (a_0, a_i, and b_i) are calculated to provide the minimum and maximum of the torsion potentials with allowance of a shift of the theoretical extreme angular positions. Comparisons of calculated versus experimental entropy and heat capacity data are reported by Chen et al.[32b]

4. Results and Discussion

4.1. Transition States Structures. The CBS-QB3 optimized transition state structures for R1−R9 are illustrated in Supporting

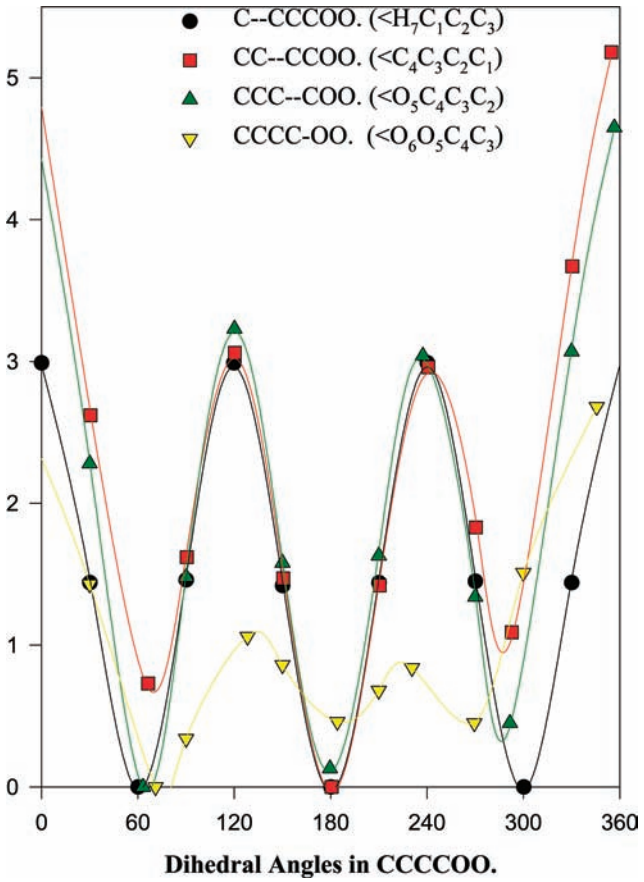

Figure 3. Potential barriers to internal rotation in CCCCOO•.

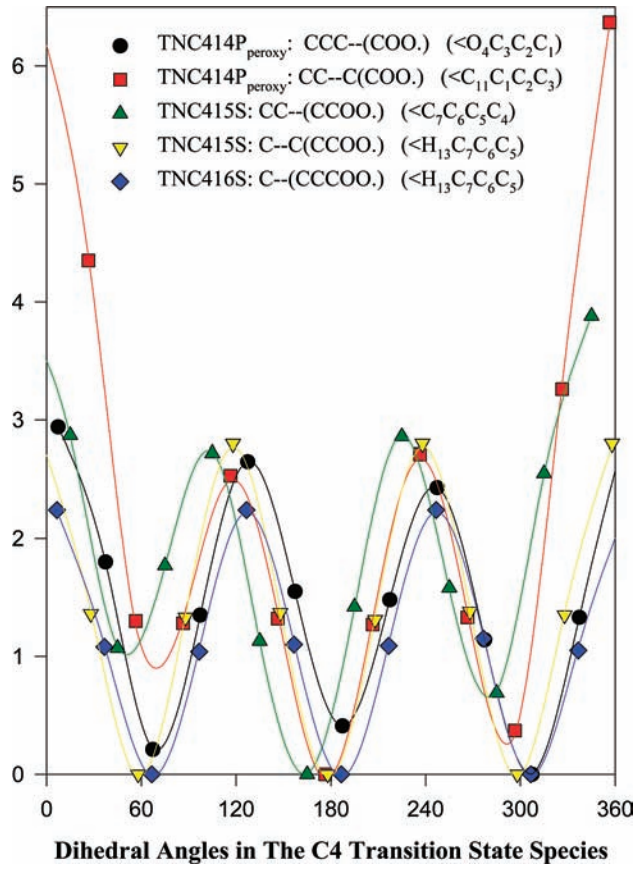

Figure 4. Potential barriers to internal rotation in 4-carbon series transition states.

TABLE 3: Enthalpies of Formation for Reference Species

species		$\Delta_f H°$(298.15 K), kcal mol^{-1}
n-propane	CCC	-25.02 ± 0.12[39]
n-butane	CCCC	-30.02 ± 0.17[39]
n-pentane	CCCCC	-35.11 ± 0.22[39]
n-$CH_3CH_2CH_2OOH$	CCCOOH	-44.77 ± 0.41[16]
n-$CH_3CH_2CH_2OO^•$	CCCOO•	-12.09[35]
$C^•H_2CH_2CH_2OOH$	C•CCOOH	4.83[35]
$CH_3C^•HCH_2OOH$	CC•COOH	2.62 ± 1.29[16]
CH_3CHO	CC=O	-39.70 ± 0.12[39]
OH		8.91[40]

Information Table S1. Harmonic vibration frequencies and the moments of inertia calculated at the same level of theory are shown in Supporting Information Table S2. The vibrations correspond to hindered internal rotors (internal rotational barrier less than 5 kcal mol^{-1}) are noted in bold. The total energies at 298 K and zero-point vibration energies are listed in Supporting Information Table S3.

4.2. Selection of Most Stable Rotational Isomer(s). We selected a zigzag (∧∧∧∧∧) backbone for the linear *n*-C_4H_9-$OO^•$ and *n*-$C_5H_{11}OO^•$ alkyl peroxy radicals ($ROO^•$) and the corresponding $R'C^•OOH$ products as the initial geometry for optimization at B3LYP/6-31G(d,p) calculation level. Internal rotor potentials were then scanned (relaxed scan) at the same level. When a lower energy conformer was identified, we re-evaluate the internal rotors previously scanned to see if a lower conformer can result. We continue this until we find no lower energy structures.

These internal rotation scans revealed the presence of lower energy conformers. One example, a conformer of $CCCCOO^•$ that has dihedral angles ∠OC−CC and ∠OO−CC around 60° is 0.69 kcal mol^{-1} in lower in energy than the zigzag conformer at B3LYP/6-31G(d,p) level. This difference is further confirmed to be 0.14 and 0.65 kcal mol^{-1} at B3LYP/6-311++G(2d,p)//B3LYP/6-31G(d,p) and CBS-QB3 levels, respectively. Although the differences are small, the zigzag conformer for this $CCCCOO^•$ peroxy radical is not its lowest conformer according to the calculation the methods we have used.

To compare the consistency of the three calculation methods, we list the results for several the lower energy rotational isomers (rotamers) for each of the C_4 compounds in Table 1 and a more complete listing in Supporting Information Table S6. In the three isomers of $CCCCOO^•$, we identify rotamer "C" (TGG, see Supporting Information Table S6) as the lowest energy one (Table 1). For some compounds, the three calculation methods give the same order of stability: for example in $CCCCOO^•$, all three methods show same C (TGG) < B (TGT) < A (TTT). This is also seen for $TnC_4$15S and $TnC_4$17P. In some cases, however, the three methods predict different orders of stability, examples are $C^•CCCOOH$ and $CC^•COOH$. We choose the isomers that have the lowest energy at CBS-QB3 level, because CBS-QB3 is the highest calculation level used. For species in the C4 series the B3LYP/6-31G(d,p) level shows slightly better consistency in energy trends with CBS-QB3 than the B3LYP/6-311++G(2d,p) level.

A complete analysis on all $CCCCOO^•$ rotamers is shown in Supporting Information Table S6. The lowest energy one at CBS-QB3 level has the TGG form, which is same as the rotamer C for $CCCCOO^•$ described above.

The optimization structures of the most stable isomers of the reactants and products in R1−R9 are illustrated in Supporting Information Table S4.

The calculated $\Delta_f H°$(298 K) values for the lowest energy conformer of the reactants and products at each of the three calculation levels are listed in Table 2, where the CBS-QB3

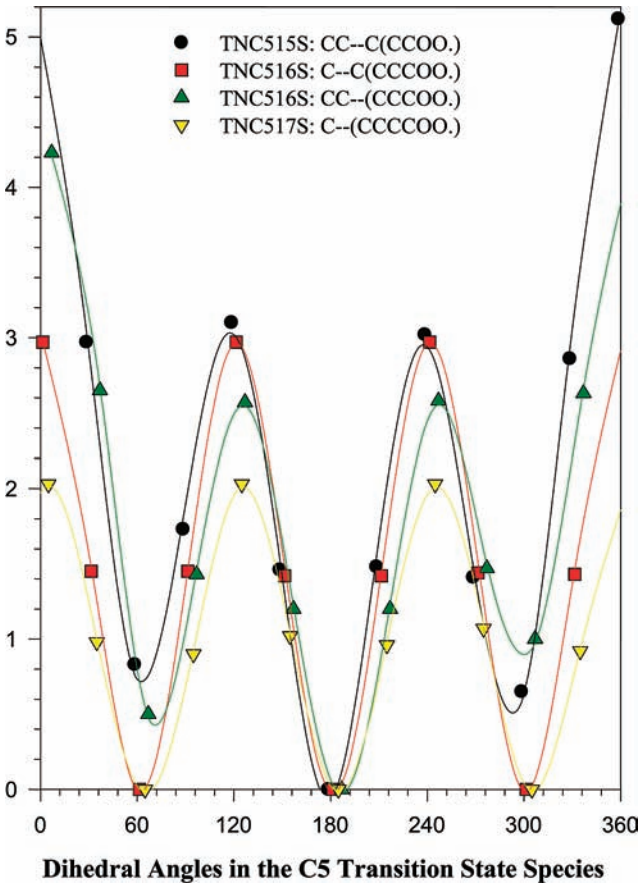

Figure 5. Potential barriers to internal rotation about C−C or C−O bonds in *n*-pentyl peroxy transition states.

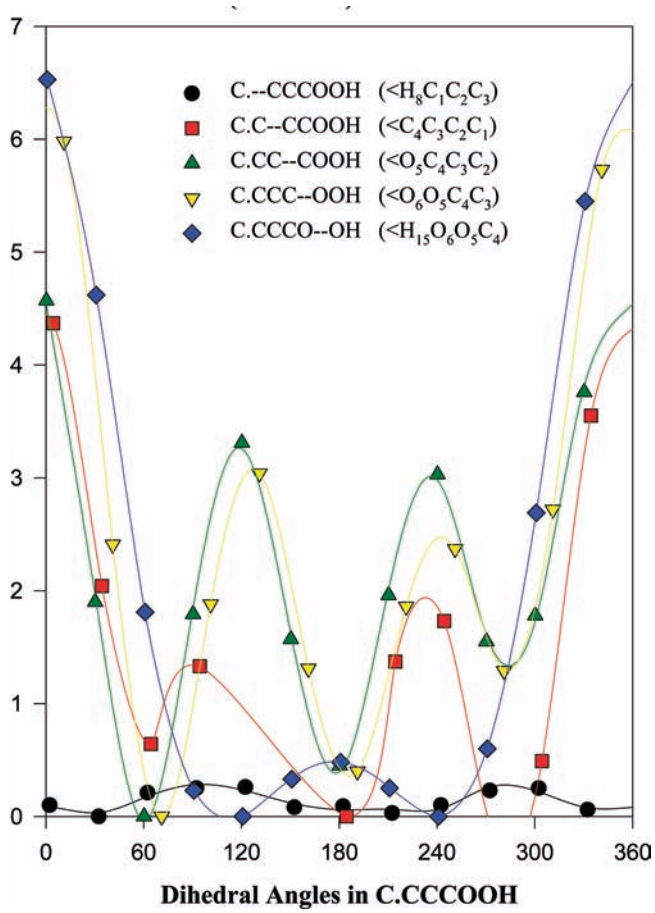

Figure 6. Potential barriers to internal rotation in C•CCCOOH.

values are recommended. The enthalpies of formation for the reference species used in these isodesmic reactions are summarized in Table 3. Overall, the agreement on the $\Delta_f H°$(298 K) values from the three calculation methods is excellent and shows that the B3LYP DFT methods with isodesmic reaction analysis are suitable for enthalpy values of these hydroperoxide and peroxy molecules and radicals.

When the radical site is on the α-carbon of an alkyl hydroperoxide, i.e., RC•OOH, the radical rapidly dissociates to the corresponding aldehyde (RCH═O) + OH due to exothermicity of the reaction (∼35 kcal mol^{-1}). This occurs via cleavage of the weak C•O−OH bond (45) and formation of the strong (∼80) carbonyl π bond, with a negligible (0−4 kcal mol^{-1}) barrier. Calculated $\Delta_f H°$(298 K) of corresponding CCCC═O and CCCCC═O aldehydes are included in Table 2 in place of CCCC•OOH and CCCCC•OOH.

All of the 5-, 6-, 7-, and 8-member-ring structures in these transition states have two conformers. One conformer is calculated to be 0.4−2.2 kcal mol^{-1} more stable at the CBS-QB3 level. The conformer that has the lower energy is used. The 4-member-rings in TnC_414P_{perox} and TnC_514S are near planar and the rings have only one structure

The potential energy diagrams for intramolecular H-abstraction reactions in CCCCOO• and CCCCCOO• are shown in Figures 1 and 2, where the data for stable species and TS shown are absolute enthalpies of formation at 298 K.

4.3. Internal Rotation Barriers. Figure 3 shows the energy profile of the four internal rotations in the *n*-butyl peroxy radical CCCCOO•. The internal rotation calculations for the transition species, TCCC(COO•), TCC(CCOO•), and TC(CCCOO•), are illustrated in Figure 4. The internal rotational barrier of TC−CC(COO•) is not computed and assumed to be the same as C−CCCOO• because of the similar structures around the internal rotation axis. The computations for some of the internal rotors in the C_5 transition state species are shown in Figure 5. During the scan of the internal rotors for transition state structures (TSs), the ring structure in the TSs is frozen while the rest of molecule structure is optimized.

Similar diagrams are shown in Figures 6−8 for C•CCCOOH, CC•CCOOH, and CCC•COOH, respectively.

Four of the five internal rotor potentials in *n*-C_4H_9OOH are illustrated in Figure 9. The internal rotational barrier of C−CCCOOH is not computed and assumed to be the same as C−CCCOO•. The internal rotation potentials in *n*-pentyl peroxide, CCCCCOOH, are assumed to be the same as those in CCCCOOH and CCCCOO•.

The thermochemical parameters of all the species in this study are listed in Table 4, where the contribution from each internal rotor to $S°(298)$ and $C_p°(T)$ are indicated. Results from our group additivity method[32−34] are also compared in this table and show reasonable agreement with the calculated values.

4.4. Bond Dissociation Energies. The C−H bond dissociation energies, obtained from data in Table 2, for *n*-C_4H_9OOH and *n*-$C_5H_{11}OOH$ are illustrated in Figure 10. The corresponding bond energies are almost identical for the respective primary C−H, or secondary C−H bonds in the two hydroperoxides.

The ROO−H bond dissociation energy in R = *n*-C_4H_9OOH and *n*-$C_5H_{11}OOH$ is 84.7 kcal mol^{-1}, which is ca. 1 kcal mol^{-1} weaker than in the methyl hydroperoxide. The bond energies in CH_3OO-H, CH_3CH_2OO-H, and $CH_3CH_2CH_2-OO-H$ are 86.05,[24] 85.10,[24] and 84.78[35] kcal mol^{-1}, respec-

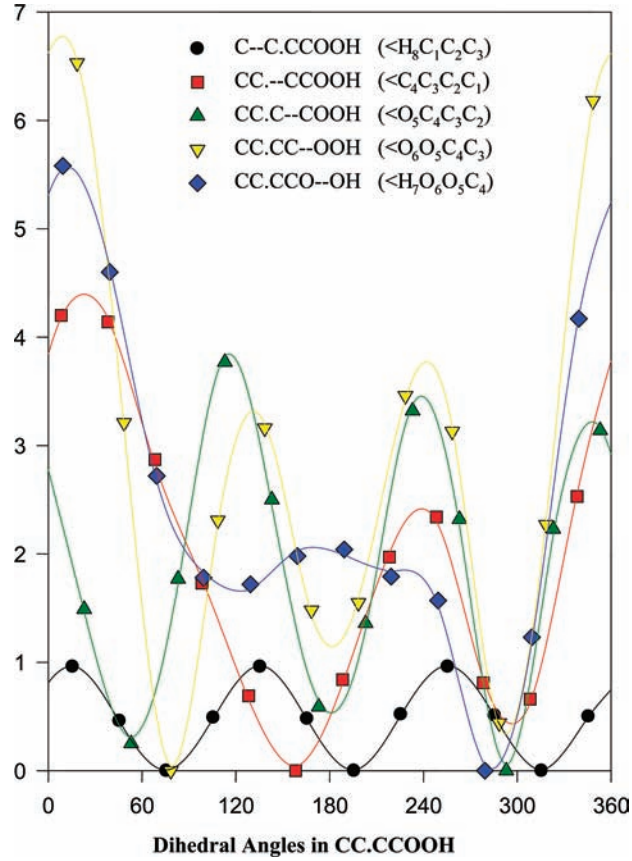

Figure 7. Potential barriers to internal rotation in CC•CCOOH.

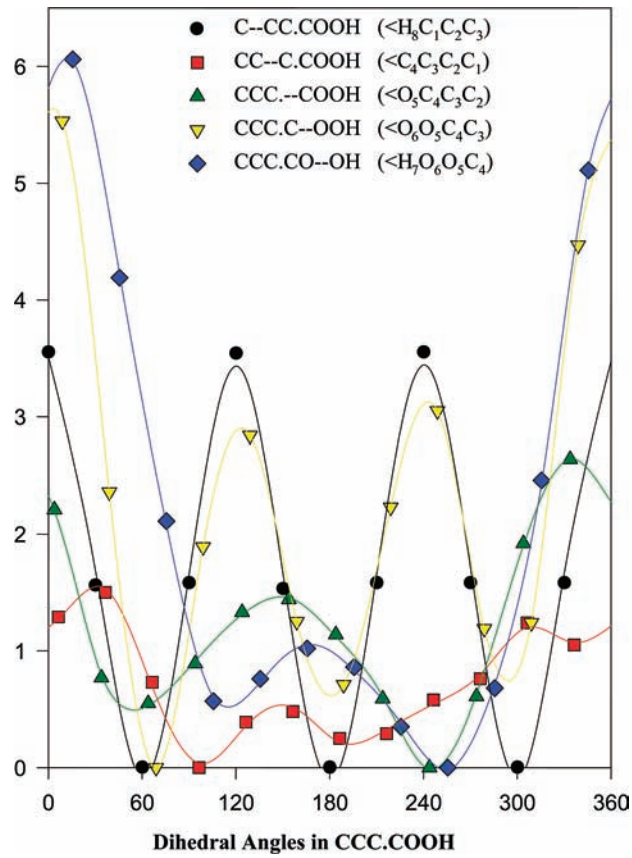

Figure 8. Potential barriers to internal rotation in CCC•COOH.

tively. Our data support the difference of the ROO−H bond energy between the methylhydroperoxide and that of the higher hydrocarbons.

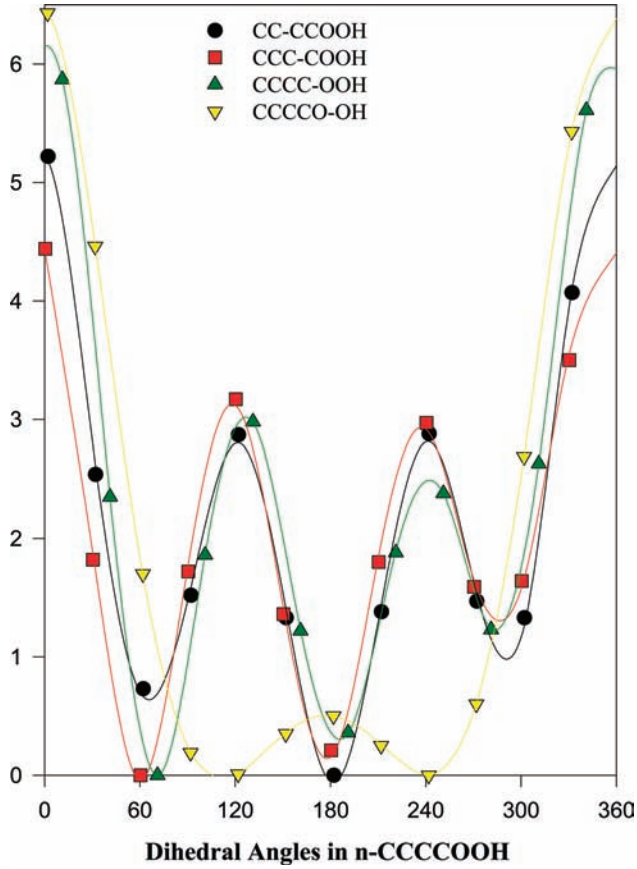

Figure 9. Potential barriers to internal rotation in CCCCOOH.

The H's on primary carbons are the most strongly bound in these hydroperoxides; the bond energy is 101.8−101.9 kcal mol^{-1}, near 1 kcal mol^{-1} stronger than the 101.1 kcal mol^{-1} C−H bond on a normal, ethyl primary carbon. The C−H on the unique secondary carbon that is adjacent to the −CH(−H)-COOH group (CH_2− bonded to the −COOH group), has 1.2−1.3 kcal mol^{-1}stronger C−H bond than a normal secondary, 99.6−99.7 kcal mol^{-1} (see Figure 10). This is attributed to electrostatic effects, the partially positive charge on the carbon of the −COOH group draws electron from the adjacent carbon making its bonds to electron donating groups (hydrogen or carbon in this peroxide system) stronger.

The C−H bond on the carbon bonding the peroxy or hydroperoxide group on the RCH(−H)OOH is ∼95 kcal mol^{-1} (according to our unpublished MP2 calculations on CH_3OOH, CCOOH, and CCCCOOH). This is weaker than a normal secondary C−H (98.4), and it may, therefore, undergo abstraction more readily. The abstraction of this H-atom might also be influenced by the exothermicity of the ensuing reaction: RC•HOOH → RCH═O + OH ($\Delta_{rxn}H = -34$ kcal mol^{-1}).

$$CH_3CH_2OO \rightarrow TST \rightarrow [CH_3C^{\bullet}H(OOH)]^* \qquad \Delta_{rxn}H = 9 \text{ kcal mol}^{-1}$$

and

$$[CH_3C^{\bullet}H(OOH)]^* \rightarrow CH_3CH{=}O + OH \qquad \Delta_{rxn}H = -35 \text{ kcal mol}^{-1}$$

There is no barrier for the $CH_3C^{\bullet}H(OOH)$ dissociation to acetaldehyde + OH at the CBS-QB3 calculation level.

TABLE 4: Calculated Ideal Gas-Phase Thermochemical Properties[a,b]

				$C_p°(T)$							
		$\Delta_f H°$(298 K)	$S°$(298 K)	300 K	400 K	500 K	600 K	800 K	1000 K	1500 K	note
CCCCOOH	TVR[c]		81.74	25.64	33.00	39.87	45.77	55.02	61.85	72.45	
	CCC-CQ		6.68	2.56	2.45	2.26	2.07	1.75	1.54	1.27	*d*
	C-CCCQ		4.40	2.16	2.15	2.03	1.87	1.61	1.44	1.22	*e*
	total	−49.74	92.82	30.36	37.60	44.16	49.71	58.38	64.83	74.94	
	THERM[l]	−49.65	94.46	31.29	38.62	44.97	50.42	58.74	65.19		
CCCCOO•	TVR		75.23	21.49	28.51	35.07	40.71	49.55	56.01	65.91	
	CCCC−OO		7.05	1.84	1.62	1.49	1.39	1.27	1.19	1.10	*d*
	CCC−COO		6.87	2.15	2.13	2.04	1.92	1.70	1.52	1.28	*d*
	C−CCCOO		4.40	2.16	2.15	2.03	1.87	1.61	1.44	1.22	*d*
	total	−17.14	93.55	27.63	34.42	40.63	45.90	54.13	60.16	69.50	
	THERM[l]	−13.55	94.68	29.24	35.78	41.42	46.33	54.02	60.22		
$TnC_4$14P_{peroxy}	TVR		81.50	23.43	30.58	37.11	42.66	51.26	57.48	66.85	
	CCC−(COO•)		6.87	2.44	2.20	1.96	1.77	1.50	1.34	1.16	*d*
	C−CC(COO•)		4.38	2.15	2.15	2.03	1.87	1.61	1.44	1.22	*e*
	total	23.71	92.75	28.03	34.94	41.10	46.30	54.37	60.26	69.23	
$TnC_4$15S	TVR		77.61	22.61	30.08	36.84	42.54	51.27	57.52	66.89	
	CC−(CCOO•)		6.31	3.07	2.66	2.31	2.04	1.68	1.47	1.22	*d*
	C−C(CCOO•)		4.49	2.16	2.12	1.97	1.81	1.56	1.39	1.19	*d*
	total	14.40	88.40	27.84	34.86	41.12	46.39	54.50	60.38	69.30	
$TnC_4$16S	TVR		79.11	24.22	31.85	38.71	44.48	53.27	59.54	68.91	
	C−(CCCOO•)		4.76	2.12	1.95	1.76	1.60	1.39	1.27	1.12	*d*
	total	3.32	83.87	26.34	33.80	40.47	46.08	54.66	60.81	70.03	
$TnC_4$17P	total	5.54	81.39	25.75	33.72	40.74	46.57	55.38	61.63	70.95	
C•CCCOOH	TVR		77.21	24.08	31.13	37.41	42.69	50.83	56.10	66.14	
	C•CC−COOH		6.64	3.21	3.01	2.66	2.33	1.85	1.57	1.26	*d*
	C•C−CCOOH		6.57	2.21	2.11	1.99	1.87	1.65	1.49	1.27	*d*
	C•−CCCOOH		4.75	1.51	1.41	1.31	1.25	1.16	1.11	1.05	*d*
	total	−0.05	95.17	31.01	37.66	43.38	48.13	55.49	60.27	69.72	
	THERM[l]	−0.65	97.87	30.52	37.26	43.06	48.02	55.58	61.45		
CC•CCOOH	TVR		77.48	23.73	30.70	37.00	42.35	50.65	56.75	66.18	
	CC•C−COOH		6.82	2.46	2.34	2.18	2.00	1.71	1.51	1.26	*d*
	CC•−CCOOH		6.49	2.20	2.12	2.00	1.88	1.66	1.50	1.27	*d*
	C−C•CCOOH		5.48	1.45	1.29	1.19	1.14	1.08	1.05	1.02	*d*
	total	−3.14	96.27	29.84	36.45	42.37	47.37	55.10	60.81	69.73	
	THERM[l]	−3.30	98.90	29.79	36.29	41.87	47.03	54.99	60.74		
CCC•COOH	TVR		77.35	23.92	30.87	37.13	42.43	50.64	56.68	66.08	
	CCC•−COOH		7.71	2.34	1.93	1.68	1.51	1.32	1.21	1.10	*d*
	CC−C•COOH		7.65	1.66	1.44	1.31	1.22	1.13	1.09	1.04	*d*
	C−CC•COOH		4.20	2.10	2.21	2.15	2.03	1.78	1.58	1.30	*d*
	total	−2.20	96.91	30.02	36.45	42.27	47.20	54.86	60.55	69.51	
	THERM[l]	−3.30	97.53	30.68	37.07	42.69	47.61	55.20	61.14		
CCCC═O	TVR		71.34	19.22	25.00	30.52	35.34	43.06	48.78	57.57	
	CCC−C═OH		6.07	3.20	2.31	1.82	1.55	1.29	1.17	1.07	*d*
	C−CCC═OH		4.35	2.15	2.16	2.04	1.89	1.63	1.45	1.22	*d*
	total	−49.82	81.77	24.57	29.47	34.38	38.78	45.98	51.40	59.86	
	THERM[l]	−49.30	82.02	24.92	30.36	35.17	39.32	46.39	51.51		
CCCCCOOH	TVR		89.14	30.53	39.48	47.82	55.00	66.26	74.54	87.35	
	CCCC−COOH		6.96	2.94	2.73	2.46	2.21	1.83	1.59	1.29	*f*
	C−CCCCOOH		4.41	2.16	2.16	2.03	1.87	1.61	1.44	1.22	*e*
	total	−54.96	100.51	35.63	44.37	52.31	59.08	69.70	77.57	89.86	
	THERM[l]	−54.65	103.86	36.79	45.57	53.22	59.77	69.81	77.53		
CCCCCOO•	TVR		82.97	26.45	35.01	43.04	49.95	60.78	68.70	80.81	
	CCCCC−OO		7.08	1.85	1.63	1.49	1.39	1.27	1.19	1.10	*d*
	CCCC−COO		7.18	2.43	2.35	2.21	2.05	1.77	1.57	1.30	*d*
	C−CCCCOO		4.41	2.16	2.16	2.03	1.87	1.61	1.44	1.22	*d*
	total	−22.37	101.64	32.89	41.14	48.77	55.27	65.43	72.90	84.42	
	THERM[l]	−18.55	104.08	34.74	42.73	49.67	55.68	65.09	72.56		
$TnC_5$14P_{peroxy}	TVR		89.28	28.37	37.09	45.09	51.92	62.50	70.17	81.76	
	CCCC−(COO•)		7.27	2.45	2.21	1.97	1.77	1.50	1.34	1.16	*g*
	C−CCC(COO•)		4.41	2.16	2.16	2.03	1.87	1.61	1.44	1.22	*e*
	total	18.44	100.96	32.98	41.45	49.08	55.56	65.61	72.95	84.14	
$TnC_5$15S	TVR		84.86	27.49	36.53	44.77	51.75	62.48	70.19	81.78	
	CCC−(CCOO•)		6.78	3.00	2.64	2.31	2.04	1.68	1.47	1.22	*h*
	C−CC(CCOO•)		4.41	2.16	2.16	2.03	1.87	1.61	1.44	1.22	*e*
	total	9.13	96.05	32.65	41.32	49.10	55.66	65.77	73.10	84.22	
$TnC_5$16S	TVR		82.65	27.18	36.40	44.74	51.77	62.53	70.24	81.81	
	CC−(CCCOO•)		6.47	2.87	2.50	2.19	1.96	1.64	1.45	1.22	*d*
	C−C(CCCOO•)		4.42	2.16	2.15	2.02	1.87	1.61	1.43	1.21	*d*
	total	−2.35	93.53	32.20	41.05	48.95	55.59	65.78	73.12	84.25	
$TnC_5$17S	TVR		84.68	29.19	38.41	46.76	53.79	64.57	72.29	83.86	
	C−(CCCCOO•)		4.87	2.07	1.87	1.67	1.52	1.33	1.22	1.10	*d*
	total	−3.01	89.55	31.26	40.28	48.43	55.31	65.90	73.51	84.96	

TABLE 4: Continued

				$C_p°(T)$							
		$\Delta_f H°$(298 K)	$S°$(298 K)	300 K	400 K	500 K	600 K	800 K	1000 K	1500 K	note
$TnC_5$18P		1.45	88.02	30.87	40.37	48.83	55.90	66.67	74.36	85.87	
C•CCCCOOH	TVR		89.81	31.22	39.78	47.50	54.02	64.14	71.55	83.06	
	C•CCC−COOH		7.28	2.54	2.37	2.17	1.99	1.70	1.51	1.26	*f*
	C•−CCCCOOH		5.17	1.01	1.01	1.00	1.00	1.00	1.00	0.99	*d*
	total	−5.21	102.25	34.77	43.15	50.67	57.01	66.84	74.05	85.31	
	THERM[l]	−5.65	107.27	36.02	44.21	51.31	57.37	66.65	73.79		
CC•CCCOOH	TVR		81.74	28.22	36.93	44.80	51.46	61.80	69.36	81.04	
	CC•CC−COOH		6.90	3.34	3.12	2.75	2.40	1.89	1.59	1.27	*i*
	CC•−CCCOOH		6.62	1.93	1.85	1.82	1.78	1.67	1.54	1.32	*d*
	C−C•CCCOOH		5.51	1.42	1.26	1.18	1.12	1.07	1.04	1.02	*d*
	total	−8.66	100.78	34.90	43.16	50.55	56.76	66.42	73.54	84.65	
	THERM[l]	−8.30	108.30	35.29	43.24	50.12	56.38	66.06	73.08		
CCC•CCOOH	TVR		81.28	26.72	35.24	43.01	49.62	59.90	67.45	79.09	
	CCC•C−COOH		7.35	2.47	2.36	2.19	2.01	1.72	1.51	1.26	*j*
	CCC•−CCOOH		7.01	2.00	1.98	1.93	1.85	1.67	1.52	1.29	*d*
	CC−C•CCOOH		7.39	2.03	1.68	1.48	1.35	1.22	1.15	1.07	*d*
	C−CC•CCOOH		4.45	2.16	2.14	2.00	1.85	1.59	1.42	1.21	*d*
	total	−8.13	107.47	35.38	43.40	50.61	56.68	66.09	73.04	83.90	
	THERM[l]	−8.30	108.30	35.29	43.24	50.12	56.38	66.06	73.08		
CCC•CCOOH	TVR		84.55	28.87	37.38	45.11	51.67	61.87	69.37	80.98	
	CCCC•−COOH		8.07	2.33	1.97	1.71	1.54	1.33	1.22	1.10	*d*
	CCC−C•COOH		8.04	1.77	1.52	1.37	1.27	1.16	1.11	1.05	*d*
	C−CCC•COOH		4.43	2.16	2.14	2.01	1.85	1.59	1.42	1.21	*d*
	total	−7.35	105.09	35.13	43.01	50.20	56.33	65.96	73.12	84.34	
	THERM[l]	−8.30	106.93	36.18	44.02	50.94	56.96	66.27	73.48		
CCCCC=O	TVR		79.07	24.10	31.45	38.44	44.55	54.26	61.45	72.46	
	CCCC−C=OH		6.21	3.20	2.31	1.82	1.55	1.29	1.17	1.07	*k*
	C−CCCC=OH		4.40	2.16	2.16	2.03	1.87	1.61	1.44	1.22	*e*
	total	−54.99	89.69	29.46	35.92	42.29	47.98	57.16	64.06	74.75	
	THERM[l]	−54.30	91.42	30.42	37.31	43.42	48.67	57.46	63.85	60.05	
OH		8.91	43.88	7.17	7.08	7.06	7.06	7.15	7.33	7.87	

[a] $\Delta_f H°$(298 K), in kcal mol^{-1}; $S°$(298 K) and $C_p°(T)$ in cal/(mol K); [b] Internal rotors are calculated at the B3LYP/6-31G(d,p) level. [c] TVR = contributions from translational + vibrational + rotational. [d] Internal rotational barrier is calculated in this work. [e] Internal rotational barriers are taken from those in CCCCOO•. [f] Internal rotational barriers are taken from those in CCCCOOH. [g] Internal rotational barriers are taken from those in $TNC_4$14P_{peroxy}. [h] Internal rotational barriers are taken from those in $TNC_4$15S. [i] Internal rotational barriers are taken from those in C•CCCOOH. [j] Internal rotational barriers are taken from those in CC•CCOOH. [k] Internal rotational barriers are taken from those in CCCC=O. [l] THERM, a modified group additivity method.

4.5. Reaction Barriers for Intramolecular H-Abstraction Reactions. The CBS-QB3 reaction barriers are illustrated in Figures 1 and 2, and compared with B3LYP methods at two basis set levels and with the BhandHLYP/6-311G(d,p) calculations in Table 5. The $\Delta H^{\ddagger}$'s calculated by the B3LYP/6-311++G(2d,p) show better agreement with the CBS-QB3 method than the B3LYP/6-31G(d,p) method. Overall, the B3LYP/6-311++G(2d,p) results are up to 2 kcal mol^{-1} higher than those from CBS-QB3, with very good agreement for the larger (ring size), lower barrier, reactions. The $\Delta H^{\ddagger}$'s from the CBS-QB3 calculation are recommended.

The results from the BhandHLYP/6-311G(d,p) calculations, this study and the Pritchard group,[11] are consistently 5−8 kcal mol^{-1} higher than the CBS-QB3 results and are considered unsuitable for this type of reaction, without an adjustment. This is consistent with Pritchard's recommendation of reducing the BHandH values by ∼6 kcal mol^{-1}.

Data in Table 5 and in Figures 1 and 2 illustrate that the intramolecular H-transfer barriers in these linear alkyl peroxy radicals are sensitive to both the ring size up to 6-member rings, and to the C−H bond energies (ΔH_{rxn}). As an example, the $\Delta H^{\ddagger}$ is 22.7 for the abstraction from a primary carbon on *n*-butyl peroxy radical, and the $\Delta H^{\ddagger}$ is 19.4 kcal mol^{-1} for abstraction from a secondary carbon on *n*-pentyl peroxy radical, where both systems are 7-member rings. The secondary *n*-pentyl system is ∼3.4 kcal mol^{-1} lower in both endothermicity and barrier. The barriers for abstraction of a secondary C−H, decrease significantly in moving from a 4- to 5- to 6-member-ring TS structure; however, there is little change in barrier between a 6- and 7-member ring. The $\Delta H^{\ddagger}$ for 4P_{perox} reaction is 40.9 kcal mol^{-1}; it decreases to 31.5 for 5S type and further decreases to 20.5 and 19.4 kcal mol^{-1} in the 6S and 7S reactions, at the CBS-QB3 level. The $\Delta H^{\ddagger}$ shows little change (less than 0.5 kcal mol^{-1}) for corresponding reactions in the nC_4 and nC_5 systems.

A number of previously reported activation energies for these intramolecular H-shift reactions, from experiment and from calculation, are included in Table 5; they correspond to the 4P_{perox}, 5S, 6S, 6P, and 7P reactions. The reported literature values show similar $\Delta H^{\ddagger}$ values to data calculated in this study, with the BHandHLYP values consistently high.

4.6. Three-Parameter-Fit Rate Constants (without H-Tunneling). High-pressure rate constant parameters, forward and reverse, are determined using canonical transition state theory and the thermochemical parameters determined in this work. The torsion frequencies where barriers are ≤5 kcal mol^{-1} are replaced by analysis of the internal rotator contributions for improved analysis of entropy ($S°(T)$) and heat capacity ($C_p°(T)$). It is felt that the analysis of internal rotation contributions to the thermochemical parameters is important to calculation of the rate constants due to loss of significant number of internal rotors in the varied transition states structures.

The rate constants of all the reactions in this study are fitted to a three-parameter modified Arrhenius equation, $k = AT^n \exp(-\Delta H^{\ddagger}/RT)$, over the temperature range 200−1500 K using THERMKIN[27,36] program and the thermochemical parameters in Table 4, which represent a canonical transition state analysis

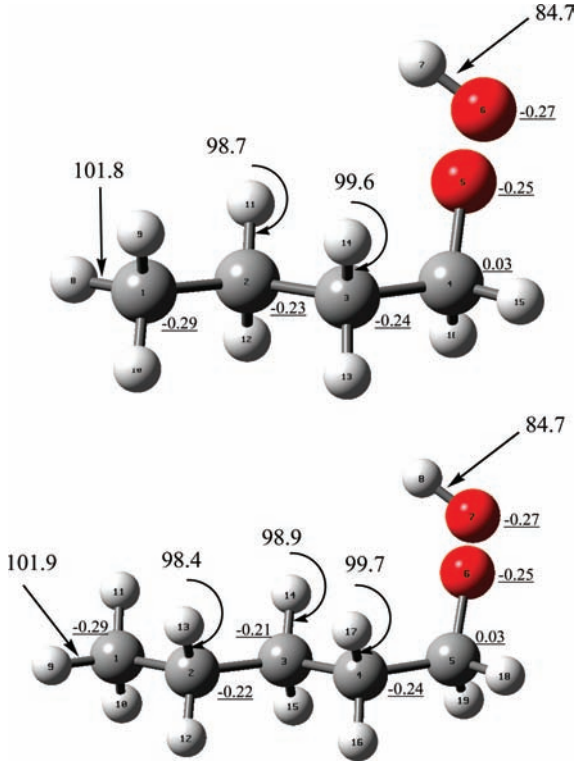

Figure 10. Calculated bond dissociation energies (kcal mol^{-1}) at the CBS-QB3 level. Underlined data are Mulliken charges. C−H bond energies on the peroxy carbon are significantly (∼3.5 kcal mol^{-1}) lower, and C−H bonds on the carbon adjacent to the peroxy carbon are ∼1 kcal mol^{-1} higher than normal secondary BE's. Primary (methyl) C−H bonds appear to be close to 102 kcal mol^{-1}, near 1 kcal mol^{-1} higher than that of ethane.

for the rate constant from the thermochemical data on the reactants and corresponding saddle point. These rate constants are listed in Table 6 and do not include tunneling effects.

4.7. Correction of Rate Constants for Hydrogen Atom Tunneling. Tunneling of the hydrogen atom is considered using Wigner's method[37] and applied to the rate constant above.

$$\Gamma(T) = 1 + \frac{1}{24}\left(\frac{h\nu^{\neq}}{k_B T}\right)^2 \qquad \text{(II)}$$

The imaginary frequencies, $\nu^{\neq}$, are corrected by 0.7, as suggested by Chen and Bozzelli.[35] The calculated hydrogen tunneling factors and the corrected rate constants are listed in Supporting Information Table S5.

4.8. Three-Parameter-Fit Rate Constants with H-Tunneling. The H-tunneling-corrected rate constants for the reactions in Table S5 are multiplied into the rate constant values at the respective temperatures and then fit to a three-parameter modified Arrhenius equation ($k(T) = AT^n \exp(-E_a/RT)$) over the temperature range 300−2000 K using the "KFIT"[27] program. The resultant rate constants are listed in Table 7 along with literature data for the corresponding reactions.

The pre-exponential (A) factors and the activation energies are plotted versus the number of atoms in the transition state ring (H atom is included) at temperatures of 300 and 1000 K in Figure 11a. The pre-exponential factors decrease significantly with an increase in ring size (increased loss of internal rotation) at both of the illustrated temperatures, for the reactions in the linear C_4 and C_5 hydrocarbons. This decrease corresponds to loss of entropy (in part loss of the internal rotor(s)). The pre exponential factors for the *n*-pentyl series are observed to have

TABLE 5: Intramolecular H-Abstraction Reaction Barriers (Forward $\Delta H^{\neq}$ at 298 K, kcal mol^{-1}) vs Calculation Method[a,b] and Comparison with Literature Values

reaction (no. of atoms in the ring-like TS, type of C atom that has a H being abstracted)	B3LYP/ 6-31G(d,p)// B3LYP/6-31G(d,p) this work	B3LYP/ 6-311++G(2d,p)// B3LYP/6-31G(d,p) this work	CBS-QB3 this work	BHANDHLYP/ 6-311G(d,p) this work	BHANDHLYP/ 6-311G(d,p) ref 11, 0 K	CBS-q//B3LYP/ 6-31G(d,p) ref 9, 0 K
(R1) CCCCOO• → TnC$_4$14P$_{perox}$ → CCCC=O + OH (4P$_{perox}$)	43.2	42.7	40.9	48.8		
(R2) CCCCOO• → TnC$_4$15S → CCC•COOH (5S)	33.2	32.4	31.5	39.2		
(R3) CCCCOO• → TnC$_4$16S → CC•CCOOH (6S)	21.8	21.3	20.5	27.5		20.34
(R4) CCCCOO• → TnC$_4$17P → C•CCCOOH (7P)	23.2	22.7	22.7	28.0	29.9	25.45
(R5) CCCCCOO• → TnC$_5$14P$_{perox}$ → CCCCC=O+ OH(4P$_{perox}$)	43.2	42.7	40.8	48.8	48.8	
(R6) CCCCCOO• → TnC$_5$15S → CCCC•COOH (5S)	33.1	32.3	31.5	39.1	39.3	
(R7) CCCCCOO• → TnC$_5$16S → CCC•CCOOH (6S)	21.7	21.2	20.0	27.3	27.7	
(R8) CCCCCOO• → TnC$_5$17S → CC•CCCOOH (7S)	19.8	19.5	19.4	25.1	26.7	
(R9) CCCCCOO• → TnC$_5$18P → C•CCCCOOH (8P)	24.2	23.7	23.8	29.0	29.2	
CCOO• → CC=O + OH (4P$_{perox}$)	41.8,[14] 40.1,[15] 42.1[17]					
CCCOO• → CCC=O + OH (4P$_{perox}$)	40.8[18]					
CCCOO• → CC•COOH (5S)	31.7,[18] ∼33.5[17]					
CC(OO•)CCCCC → CC(OOH)C•CCCC (5S)	27.9[10]					
CCOO• → C•COOH (5P)	34.3 ± 2.4,[4] 30.5,[6] 37.0,[17] 36.36[14]					
C_2COO• → CC(C•)OOH (5P)	35.7[17]					
C_3COO• → C_2C(C•)OOH (5P)	32.2,[16] 28.7[5]					
CCCOO• → C•CCOOH (6P)	23.2,[18] ∼24.9[17]					
CCC(OO•)C → C•CC(OOH)C (6P)	24.34[9]					
CC(OO•)CCCCC → CC(OOH)C•CCC (6S)	22.15[10]					
CC(OO•)CCCCC → CC(OOH)CC•CC (7S)	19.35[10]					
CC(OO•)CCCCC → CC(OOH)CCC•C (8S)	22.15[10]					

[a] $\Delta H^{\neq}$ = total energy (ZPVE and thermal correction included) difference between TS and Reactant. [b] H tunneling corrections not included.

TABLE 6: Elementary Rate Constants in Modified Arrhenius Form[a,b] (Three-Parameter Fit (200−1500 K))

reaction	A (s^{-1})	n	$\Delta H^{\neq}$ (kcal mol^{-1})
(R1) CCCCOO• → (CCCC•OOH)$^{\neq}$ → CCCC=O + OH	4.60E+09	1.168	40.8
(R2) CCCCOO• → CCC•COOH	4.74E+08	1.179	31.4
(R3) CCCCOO• → CC•CCOOH	2.09E+08	0.951	20.5
(R4) CCCCOO• → C•CCCOOH	2.08E+07	1.104	22.6
(R5) CCCCCOO• → (CCCCC•OOH)$^{\neq}$ → CCCCC=O + OH	7.87E+09	1.095	40.8
(R6) CCCCCOO• → CCCC•COOH	6.46E+08	1.098	31.5
(R7) CCCCCOO• → CCC•CCOOH	2.89E+08	1.027	20.0
(R8) CCCCCOO• → CC•CCCOOH	1.05E+08	0.871	19.4
(R9) CCCCCOO• → C•CCCCOOH	1.18E+07	1.078	23.8

[a] From thermochemical parameters shown in Table 4. [b] No H-tunneling considered.

TABLE 7: Comparison of Three-Parameter Fit, Modified Arrhenius Rate Constants

	this work[a,b]			literature			
	A (s^{-1})	n	$\Delta H^{\neq}$	A (s^{-1})	n	$\Delta H^{\neq}$	
R1	1.71E+09	1.274	40.0	1.32E+9	1.37	41.59	Sheng et al.,[14] *c*
R2	3.35E+08	1.198	30.6	3.30E9	1	32.5	Buda et al.[41]
R3	6.45E+07	1.084	19.7	1E12		23.9	Baldwin et al.[5]
				5.7E8	1	25	Buda et al.[41]
R4	6.40E+06	1.237	21.9	3.98E11		30.1	Pritchard[11]
				1.25E11		23.4	Baldwin et al.[5]
				1.5E8	1	25	Buda et al.[41]
R5	3.02E+09	1.198	40.0	1.26E13		50	Pritchard[11]
R6	4.57E+08	1.117	30.6	3.16E12		39.9	Pritchard[11]
				8.71E11		32.43	Walker et al. for cyclic,[42] *d*
				1.41E12		31.79	Walker et al. for alkyl[42]
R7	9.00E+07	1.159	19.3	7.94E11		28.0	Pritchard[11]
				6.46E11		29.52	Walker et al. for cyclic,[42] *d*
				1.74E11		26.29	Walker et al. for alkyl[42]
R8	3.40E+07	0.998	18.7	3.98E11		27.0	Pritchard[11]
				1.26E11		19.1	Baldwin et al.[5]
				7.59E10		26.89	Walker et al. for cyclic,[42] *d*
				2.19E10		21.51	Walker et al. for alkyl[42]
R9	2.80E+06	1.249	23.1	1.58E11		29.2	Pritchard[11]
				1.58E11		19.6	Baldwin et al.[5]

[a] 300−1500 K. [b] H tunneling is considered. [c] For $C_2H_5OO \rightarrow CH_3CHO + OH$. [d] For cyclohexylperoxy radicals.

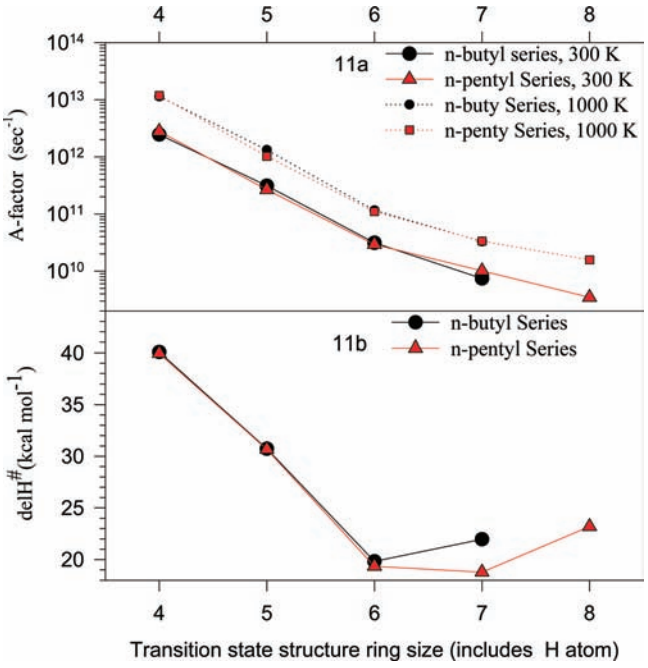

Figure 11. Pre-exponential (A) factors at 300 and 1000 K and $\Delta H^{\ddagger}$ versus number of atoms (includes H-atom) in the cyclic transition state structures.

the same values as that for the *n*-butyl system, when the number of atoms in the cyclic TS correspond.

4.9. Discussion. Figure 11b illustrates that the $\Delta H^{\ddagger}$ values are in agreement for the corresponding TS ring size in the *n*-butyl and *n*-pentyl systems, when the thermochemistry (ΔH_{rxn}) is similar. $\Delta H^{\ddagger}$ for abstraction from a secondary C−H for the 4-, 5-, and 6-member rings are near 40, 30, and 19 kcal mol^{-1}, respectively, in both series. The $\Delta H^{\ddagger}$ for 7-member ring (abstraction from a secondary carbon) in the *n*-pentyl series is ∼19 kcal mol^{-1}, which is similar (1 kcal mol^{-1} lower) than the 6-member ring in *n*-butyl series.

The $\Delta H^{\ddagger}$ for abstraction of a primary H-atom in the *n*-butyl and *n*-pentyl are also similar, ∼22 kcal mol^{-1} for *n*-butyl (7-member ring) and ∼23 kcal mol^{-1} for *n*-pentyl (8-member ring). These are abstractions of a primary methyl H-atom (CH_3 group), where the C−H bond is ∼2.5 kcal mol^{-1} stronger than a normal secondary C−H. The barriers are higher than corresponding barriers for abstraction from a secondary carbon by 2−4 kcal mol^{-1} and,, within error limits, correspond to the full difference in added endothermicity. Figure 11 demonstrates the agreement in kinetic parameters for the normal butyl and pentyl peroxy radicals when the ring size and thermochemistry of C−H hydrogen being abstracted are the similar.

Comparisons of our calculated results for reactions R1 to R9 with literature data are shown in Figures 12−20. Our calculated forward pre-exponential factors ($A_{for(T)}$) and rate constants k_{for}-(T)'s are the solid black lines, and the literature values are in color. Our calculated reverse parameters A_{rev}'s and k_{rev}'s are the dotted black lines in these figures.

Figures 12 and 16 illustrate the calculated rate constants for the 4-member-ring TS structures in the *n*-butyl (TnC_414P_{peroxy} (R1)) and *n*-pentyl (TnC_514P_{peroxy} (R5)) systems. This system is unique, as there is, effectively, is no reverse reaction because the formed R′C•(H)OOH isomer immediately dissociates to

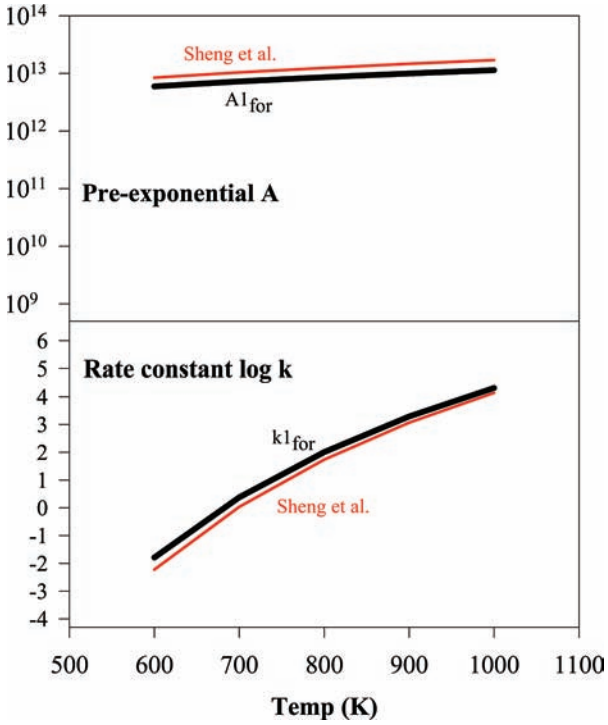

Figure 12. Pre-exponential (*A*) factor and rate constant for TnC_4-$14P_{peroxy}$ (R1). See also Table 7. Sheng et al. has the value for CCOO• → CCHO + OH.[14]

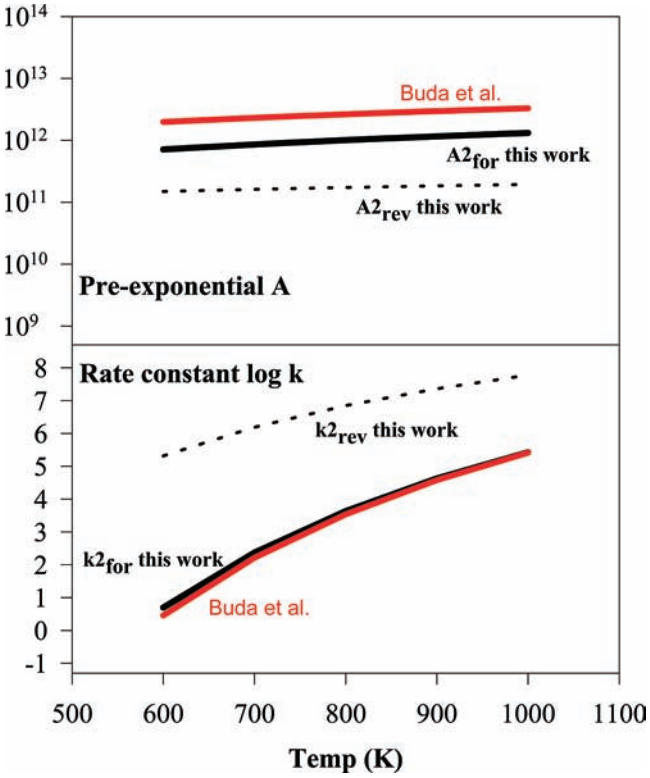

Figure 13. Pre-exponential (*A*) factor and rate constant for$TnC_4$15S (R2). See also Table 7.

lower energy products, an aldehyde (R′CH═O) + hydroxyl radical. These products are 35 kcal mol^{-1} lower in energy than the R′C•(H)OOH structure.

A comparison of kinetic parameters with data in the literature shows our pre-exponential factors for the H-atom shift to the peroxy radical site are lower than values reported in the literature for the 5-, 6-, and 7-member-ring systems. The pre-exponential

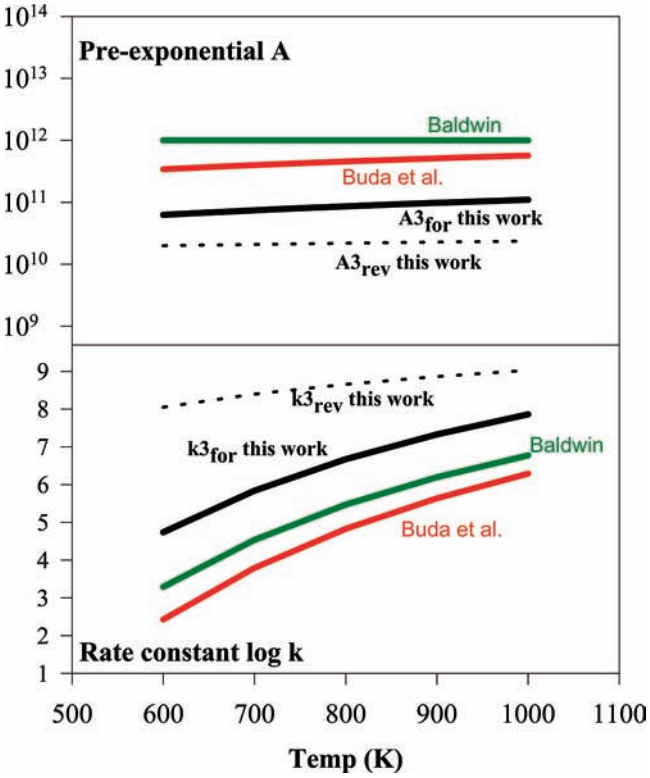

Figure 14. Pre-exponential (*A*) factor and rate constant for $TnC_4$16S (R3). See also Table 7.

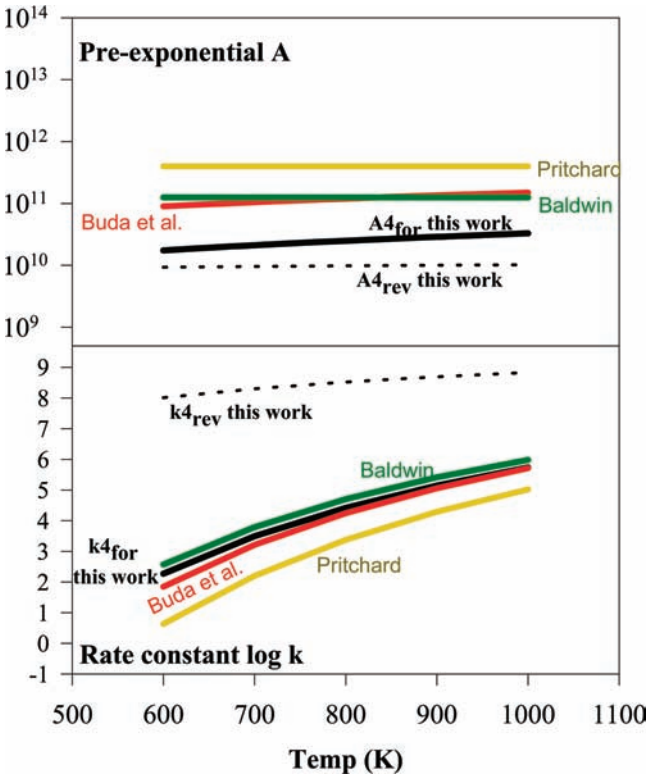

Figure 15. Pre-exponential (*A*) factor and rate constant for $TnC_4$17P (R4). See also Table 7.

factors for forward reaction in the 5-member-ring TS structures in ($TnC_4$15S (R2) Figure 13 are nearly twice as fast as the data of Buna et al., whereas data for the $TnC_5$15S (R5) 5-member-ring TS are closer to the data of the Baldwin studies, Figure 17. In both cases the forward *A* factor is about 10 times faster than the reverse *A*, but the forward rate constants (k_{for}) are more

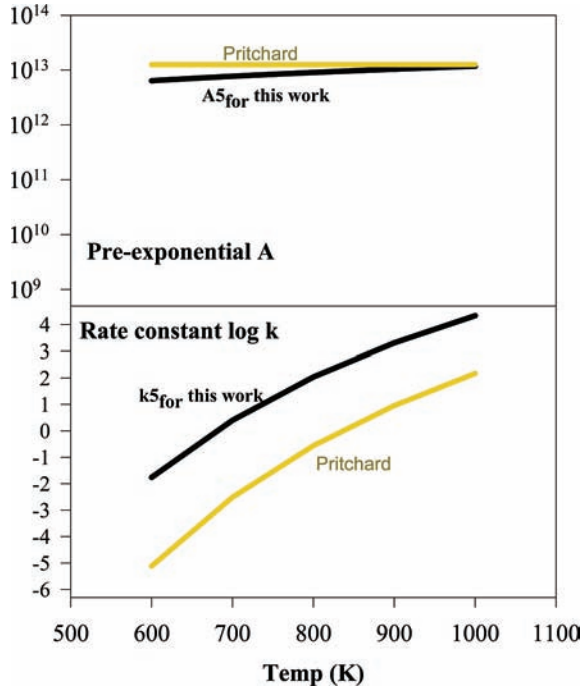

Figure 16. Pre-exponential and rate constant for $TnC_5 14P_{peroxy}$ (R5). See also Table 7.

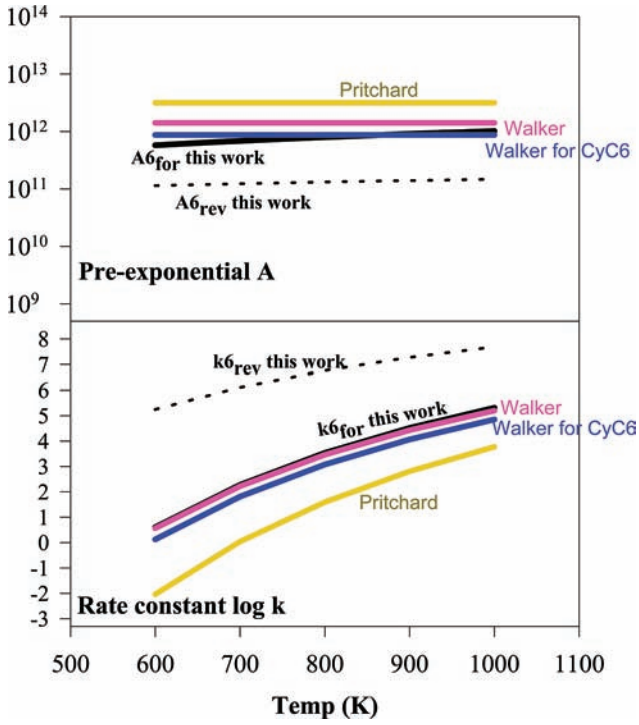

Figure 17. Pre-exponential (*A*) factor and rate constant for $TnC_5 15S$ (R6). See also Table 7.

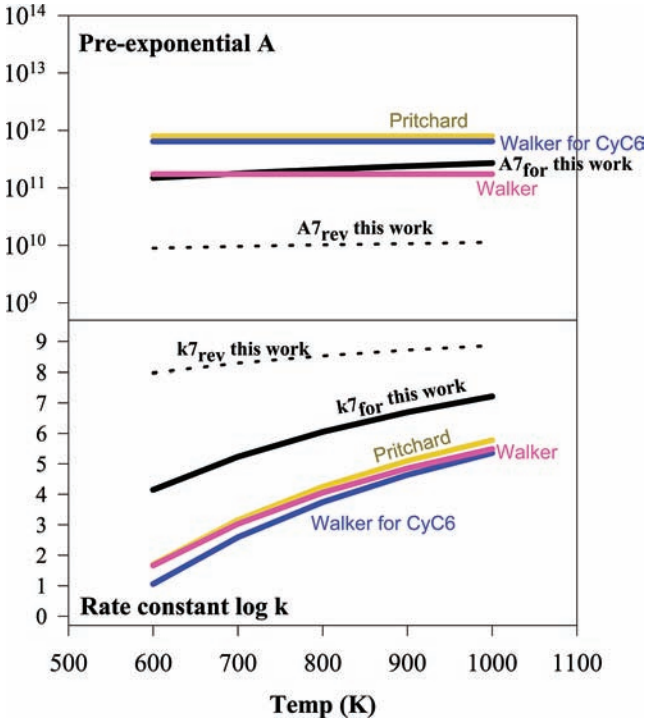

Figure 18. Pre-exponential (A) factor and rate constant for $TnC_5 16S$ (R7). See also Table 7.

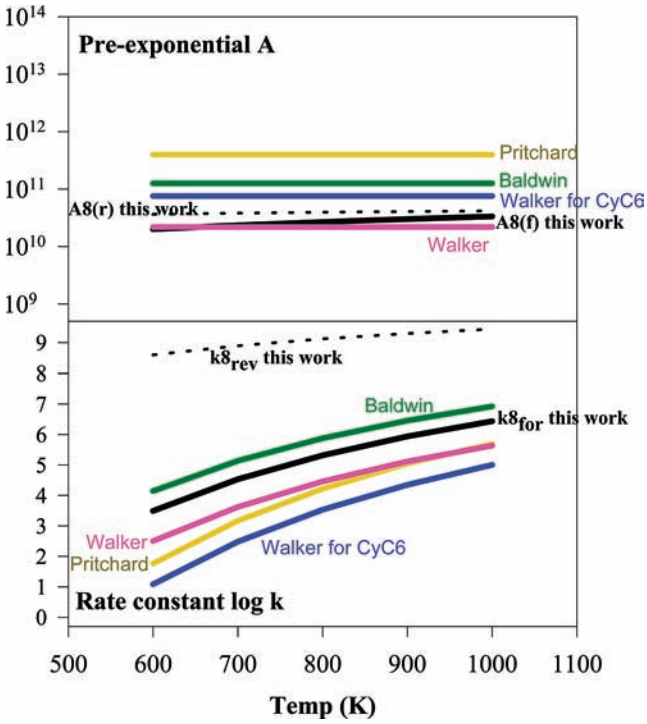

Figure 19. Pre-exponential (*A*) factor and rate constant for $TnC_5 17S$ (R8). See also Table 7.

than a factor of 100 lower than the reverse *k*'s. The difference in k_f vs k_r values is controlled by the lower reverse barriers (temperatures to 1000 K); here the $\Delta H^{\ddagger}$ is 31.5 and 16.5 kcal mol^{-1} for the respective forward and reverse reactions in the 5-member-ring TS structures.

The *A* factors for forward reaction in 6-member-ring TS, Figures 14 and 18 (*R*3 and R6), are ca. 50 times faster than the A_{rev}'s, but the overall k_{for}'s are lower than the reverse *k*'s. Here the $\Delta H^{\ddagger}$ for the reverse reaction is very low, ~6 kcal mol^{-1} whereas the $\Delta H^{\ddagger}$ for the forward reaction is ~20 kcal mol^{-1}. Our calculated forward k_3 in Figure 14 is higher than the value reported by Baldwin et al.[5] in their (550−800 K) hydrocarbon oxidation study, possibly due to neglect of the reverse reaction in the kinetic analysis.

Similar effects in pre-exponential values and forward/reverse rate constants are illustrated in Figures 15, 19, and 20 for the 7- and 8-member-ring systems.

Although comparison of kinetic parameters in the literature shows our pre-exponential *A* factors for forward reactions are overall lower than previously reported data, the rate constants for these reactions are in reasonable agreement with several

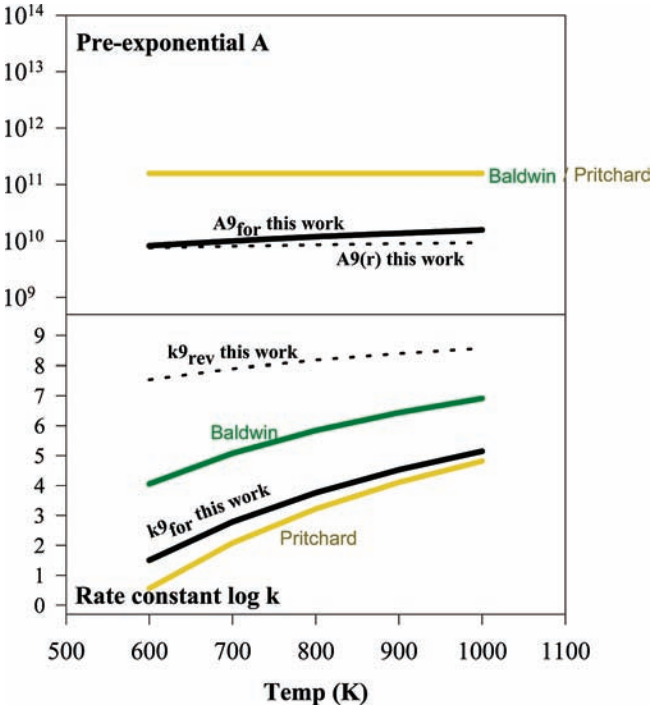

Figure 20. Pre-exponential and rate constant for $TnC_5$18P (R9). See also Table 7.

previously reported values. Agreement exists for the 4-member TS structure data with Sheng et al., the 5-member TS study of butyl by Buda et al., the 5-member TS data, and for *n*-pentyl by the Baldwin group studies, the 7-member ring in *n*-pentyl of Baldwin. We are in between the data range of two studies by the Baldwin and Walker group, on the 6-member TS in *n*-pentyl.

We find that the low pre-exponential factors result from treatment of the internal rotors in the reactant, peroxy radical and H-transfer products (hydroperoxide alkyl radicals), where internal rotor(s) are lost in the TS structure. These pre-exponential factors are even lower in the work of Broadbelt's group study[19] on branched hydrocarbons. The calculated pre-exponential factors for reactions R5 and R7 compare well with calculations of the Chan, Hamilton, and Prichard's,[11] but the overall rate constants are 1−2 orders of magnitude higher. This is expected because of the high $\Delta H^{\ddagger}$ values calculated by the BHandH method in Chan et al.'s work. The pre-exponential and the rate constant for the 7-member-ring TS ($TnC_5$17S (R8)) show good agreement with the literature.

Comparison of rate constants for the 6-member-ring H-shift in $TnC_4$16S (R3) and in $TnC_5$16S (R7) shows our values are high compared to literature values; this is a result of the calculated 20.2 kcal mol^{-1} barriers.

Our results show the reverse, H-shift, rate constants for all but the 4-member-ring transition state structures are orders of magnitude faster than the forward rate constants in the 550−800 K hydrocarbon oxidation temperature range.

4.10. Relative Concentrations of Hydroperoxide−Alkyl Radicals. The concentrations of the hydroperoxide alkyl radicals under thermal oxidation and combustion temperature conditions is expected to be lower than that of the peroxy radicals because of the low ROO−H bond energy (85 kcal mol^{-1}) relative to the RC−H bonds (98−102 kcal mol^{-1}) and the ease of the reverse H-shift. This endothermicity results in a low barrier (often less than 10 kcal mol^{-1}) to the reverse reaction. Still we find in the modeling study of Androulakis et al.[1] that the formation of these H-shift isomers are important to modeling negative temperature coefficients and low-temperature oxidation at low to moderate temperature conditions. Modeling studies of the Curran group also report that the forward H-shift forms hydroperoxides that further react to chain branching [Curran et al.[10] modeling of negative temperature effects in HC oxidation]. The intermediate alkyl radicals may, in addition, have a number of competing, low-energy, forward reactions paths, some forming strong carbonyl bonds. Although the 4-member-ring TS system in these peroxy radical H-shift reactions is unique in not having a reverse reaction, the 4-member ring reactions are not competitive with the 6- and 7-member-ring TS reactions at temperatures below 1100 K, because of the higher barrier. An experimental study to monitor the formation ratios of these hydroperoxide alkyl radicals or other specific product in these hydrogen shift reactions is difficult but would be very helpful for validation of oxidation models in this temperature regime.

5. Summary

Internal rotation barriers and thermochemical properties for *n*-butyl and *n*-pentyl hydroperoxides and the corresponding peroxy and hydroperoxide alkyl radicals, plus kinetic parameters for intramolecular H-abstraction reactions, have been evaluated using CBS-QB3 and density functional calculations. $\Delta_f H°$(298 K)'s of reactants and products are calculated using CBS-QB3 and B3LYP/6-311++G(2d,p)//B3LYP/6-31G(d,p) method with isodesmic reactions for enthalpies, and energies for the C−H bonds are determined and compared. Entropy and the heat capacities are determined from translation, vibration, rotation, and hindered internal rotation contributions. Rate constants are compared with respect to exothermicity and loss of internal rotors. The calculations at the CBS-QB3 level of computation chemistry theory support the use of B3LYP/6-311G++(2d,p) calculations, where deviations in enthalpies of conformers from the density function calculations differ by less than 1 kcal mol^{-1}. The BhandHLYP/6-311G(d,p) calculations consistently over-predict the intramolecular H-shift barriers by 6−8 kcal mol^{-1}. Rate constants for the intramolecular H-transfer are calculated and include H-tunneling estimates. Comparison of calculations for intramolecular H-transfer reactions ethyl peroxy radical (CCOO$^{\bullet}$) and propyl peroxy radical (CCCOO$^{\bullet}$) show similar pre-exponential *A* factors and barrier heights when the number of carbons in the cyclic transition state structure are the same.

Acknowledgment. We thank the Ada C. Fritts, Chair, the ExxonMobil Research and Engineering Educational fund, and the OSD/USAF Phase I and II STTR contract No's. FA8650-05-M-2615 and FA8650-06-C-2658STTR from WPAFB through Reaction Engineering International, for partial funding.

Supporting Information Available: Tables of optimized geometric parameters, vibration frequencies and moments of inertia, total energies, H-tunneling factors, and relative energies. This material is available free of charge via the Internet at http://pubs.acs.org.

References and Notes

(1) Androulakis, I. P.; Grenda, J. M.; Barckholtz, T. A.; Bozzelli, J. W. *AIChE J.* **2006**, *52*, 3246.
(2) Bozzelli, J. W.; Sheng, C. *J. Phys. Chem. A* **2002**, *106*, 1113.
(3) Androulakis, I. P.; Grenda, J. M.; Bozzelli, J. W. *AIChE J.* **2004**, *50*, 2956.
(4) Baldwin, R. R.; Pickering, I. A.; Walker, R. W. *J. Chem. Soc., Faraday Trans. 1* **1980**, *76*, 2374.
(5) Baldwin, R. R.; Hisham, W. M.; Walker, R. W. *J. Chem. Soc., Faraday Trans. 1* **1982**, *78*, 1615.

(6) Wagner, A. F.; Slagle, I. R.; Sarzynski, D.; Gutman, D. *J. Phys. Chem.* **1990**, *94*, 1853.
(7) Quelch, G. E.; Gallo, M. M.; Shen, M.; Xie, Y.; Schaefer, H. F., III; Moncrieff, D. *J. Am. Chem. Soc.* **1994**, *116*, 4953.
(8) Ignatyev, I. S.; Xie, Y.; Allen, W. D.; Schaefer, H. F., III. *J. Chem. Phys.* **1997**, *107*, 141.
(9) Jungkamp, T. P.; Smith, J. N.; Seinfeld, J. H. *J. Phys. Chem. A* **1997**, *101*, 4392.
(10) Curran, H. J.; Gaffuri, P.; Pitz, W. J.; Westbrook, C. K. *Combust. Flame* **1998**, *114*, 149.
(11) Chan, W.; Hamilton, I. P.; Pritchard, H. O. *J. Chem. Soc., Faraday Trans.* **1998**, *94*, 2303.
(12) Walker, R. W. *Spec. Period. Rep., React. Kinet.* **1975**, *1*, 161.
(13) Westbrook, C. K.; Pitts, W. J. Detailed Kinetic Modeling of Autoignition Chemistry. *SAE Tech. Paper Ser.* **1987**, 872107.
(14) Sheng, C. Y.; Bozzelli, J. W.; Dean, A. M.; Chang, A. Y. *J. Phys. Chem. A* **2002**, *106*, 7276.
(15) Carstensen, H.-H.; Naik, C. V.; Dean, A. M. *J. Phys. Chem. A* **2005**, *109*, 2264.
(16) Chen, C.-J.; Bozzelli, J. W. *J. Phys. Chem. A* **1999**, *103*, 9731.
(17) DeSain, J. D.; Klippenstein, S. J.; Miller, J. A.; Taatjes, C. A. *J. Phys. Chem. A* **2003**, *107*, 4415.
(18) Merle, J. K.; Hayes, C. J.; Zalyubovsky, S. J.; Glover, B. G.; Miller, T. A.; Hadad, C. M. *J. Phys. Chem. A* **2005**, *109*, 3637.
(19) Pfaendtner, J.; Yu, X.; Broadbelt, L. J. *J. Phys. Chem. A* **2006**, *110*, 10863.
(20) Curtiss, L. A.; Raghavachari, K.; Redfern, P. C.; Pople, J. A. *J. Chem. Phys.* **1997**, *106*, 1063.
(21) Durant, J. L. *Chem. Phys. Lett.* **1996**, *256*, 595.
(22) Durant, J. L.; Rohlfing, C. M. *J. Chem. Phys.* **1993**, *98*, 8031.
(23) Petersson, G. A.; Malick, D. K.; Wilson, W. G.; Ochterski, J. W.; Montgomery, J. A., Jr.; Frisch, M. J. *J. Chem. Phys.* **1998**, *109*, 10570.
(24) Sebbar, N.; Bockhorn, H.; Bozzelli, J. W. *Phys. Chem. Chem. Phys.* **2002**, *4*, 3691.
(25) Sebbar, N.; Bozzelli, J. W.; Bockhorn, H. *J. Phys. Chem. A* **2004**, *108*, 8353.
(26) Scott, A. P.; Radom, L. *J. Phys. Chem.* **1996**, *100*, 16502.
(27) Sheng, C. Ph.D. Dissertation, Dept. of Chemical Engineering, New Jersey Institute of Technology, 2002. PC version of the code is available by writing the authors.
(28) Shokhirev, N. V. http://www.chem.arizona.edu/faculty/walk/nikolai/programs.html#programs.
(29) Lay, T. H.; Krasnoperov, L. N.; Venanzi, C. A.; Bozzelli, J. W. *J. Phys. Chem.* **1996**, *100*, 8240.
(30) Yamada, T.; Lay, T. H.; Bozzelli, J. W. *J. Phys. Chem.* **1998**, *102*, 7286.
(31) Yamada, T.; Lay, T. H.; Bozzelli, J. W. *J. Phys. Chem.* **1999**, *103*, 5602.
(32) (a) Lay, T. H.; Bozzelli, J. W.; Dean, A. M.; Ritter, E. R. *J. Phys. Chem.* **1995**, *99*, 14514. (b) Chen, C.; Bozzelli, J. W. *J. Phys. Chem.* **2003**, ***107***, 4531.
(33) Ritter, E. R.; Bozzelli, J. W. *Int. J. Chem. Kinet.* **1991**, *23*, 767.
(34) Ritter, E. R. *J. Chem. Inf. Comput. Sci.* **1991**, *31*, 400.
(35) Chen, C.; Bozzelli, J. W. New Jersey Institute of Technology, Newark, NJ. Personal communications.
(36) Zhu, L.; Bozzelli, J. W. *Chem. Phys. Lett.* **2002**, *357*, 65.
(37) Wigner, E. P. *Z. Phys. Chem.* **1932**, *B19*, 203.
(38) da Silva, G.; Bozzelli, J. W. *J. Phys. Chem. A* **2006**, *110*, 13058.
(39) Pedley, J. B.; Naylor, R. O.; Kirby, S. P. *Thermodynamic Data of Organic Compounds*, 2nd ed.; Chapman and Hall: London, 1986.
(40) Conaire, M. O.; Curran, H. J.; Simmie, J. M.; Pitz, W. J.; Westbrook, C. K. *Int. J. Chem. Kinet.* **2004**, *36*, 603.
(41) Buda, F.; Bounaceur, R.; Warth, V.; Glaude, P. A.; Fournet, R.; Battin-Leclerc, F. *Combust. Flame* **2005**, *142*, 170.
(42) Handford-Styring, S. M.; Walker, R. W. *Phys. Chem. Chem. Phys.* **2001**, *3*, 2043.